Planetary bearing defect detection in a commercial helicopter main gearbox with vibration and acoustic emission

Faris Elasha[1*], Matthew Greaves[2], David Mba[3]

[1] Faculty of Engineering, Environment and computing, Coventry University (UK)

[2] School of Aerospace, Transport, and Manufacturing, Cranfield University (UK)

[3] Faculty of Technology, De Montfort University, (UK)

Abstract

Helicopter gearboxes significantly differ from other transmission types and exhibit unique behaviors that reduce the effectiveness of traditional fault diagnostics methods. In addition, due to lack of redundancy, helicopter transmission failure can lead to catastrophic accidents. Bearing faults in helicopter gearboxes are difficult to discriminate due to the low signal to noise ratio (SNR) in the presence of gear vibration. In addition, the vibration response from the planet gear bearings must be transmitted via a time-varying path through the ring gear to externally mounted accelerometers, which cause yet further bearing vibration signal suppression.

This research programme has resulted in the successful proof of concept of a broadband wireless transmission sensor that incorporates power scavenging whilst operating within a helicopter gearbox. In addition, this paper investigates the application of signal separation techniques in detection of bearing faults within the epicyclic module of a large helicopter (CS-29) main gearbox using vibration and Acoustic Emissions (AE). It compares their effectiveness for various operating conditions. Three signal processing techniques including an adaptive filter, spectral kurtosis and envelope analysis, were combined for this investigation. In addition, this research discusses the feasibility of using AE for helicopter gearbox monitoring.

Keywords

Helicopter Main gearbox, Acoustic Emission, signal separation, bearing diagnostics

*Corrsponding Author. Tel: +442477659139

Email: faris.elasha@coventry.ac.uk

Abbreviation

AE	Acoustic Emission
ANC	Adaptive Noise Cancelation
CAA	Civil Aviation Authority
CI	Condition Indicators
HUMS	Health and Usage Monitoring Systems
LP	Linear Prediction
MGB	Main Gearbox
ORD	Outer race Defect
SK	Spectral Kurtosis
SNR	Signal Noise Ratio
TSA	Time Synchronous Averaging
V^2rms	Voltage square root mean square

1 Introduction

Helicopter transmission integrity is critical for safe operation. Approximately 16% of mechanical failures, resulting in the loss of helicopter operation, can be attributed to the main gearbox (MGB)[1]. In addition, 30% of the total maintenance cost of helicopters can be attributed to the transmission system [1]. The need to employ advanced fault warning systems for such transmission systems cannot be understated [2, 3]. Health and Usage Monitoring Systems (HUMS) are commonly used for fault detection of helicopter transmissions in which detection is based on the extraction of predefined features of the measured vibration such as FM4, NA4, etc. [2, 4]. HUMS was developed in North Sea operations, motivated in part by the crash to a Boeing Vertol 234 in 1986 which was caused by disintegration of the forward main gearbox. After development in the 1990s, the UK's Civil Aviation Authority CAA mandated fitment of HUMS to certain helicopters. One article suggests that HUMS "successes" are found at a frequency of 22 per 100,000 flight hours [5]. A HUM system consists of two

complimentary subsystems: health monitoring and usage monitoring. Health monitoring is a process of diagnosing incipient damage or degradation that could ultimately lead to a system failure. Usage monitoring is a process by which the remaining life of different gearbox components and auxiliary systems is determined by assessing operation hours, current components condition and load history [6, 7]. In relation to health monitoring, vibration analysis methods have been developed and applied in HUMS to detect faults in bearings, gears and shafts. Condition Indicators (CI) refer to the characteristics extracted from these virations and are used to reflect the health of the component [8]. Numerous condition indicators are calculated from vibration data to characterize component health and these indicators are often determined based on statistical measurement of the energy of the vibration signal.

The majority of helicopters utilise epicyclic gear reduction modules gears as transmission systems due to their high transmission ratio, higher torque to weight ratio and high efficiency [9]. As such this type of gearbox is widely used in many industries such as aerospace, wind turbines, mining and heavy trucks [10-14]. Different planetary gearbox configurations and designs allow for a range of gear ratios, torque transmission, and shaft rotational characteristics. The planetary gearbox generally operates under severe conditions, thus, the gearbox components are subject to different kinds of fault conditions such as gear pitting, cracks, etc. [15-18]. Recent investigations on applications of planetary gearboxes have shown that failures initiate at a number of specific bearing locations, which then progress into the gear teeth. In addition bearing debris and the resultant excess clearances are known to cause gear surface wear and misalignment [18]. More recently the accident to the helicopter registred (G-REDL) [19], resulting in the loss of 16 lives, was caused by the degradation of a planet gear bearing interestingly the HUM system condition indicators showed no failure evidence before this accident.

2 Planetary gearbox diagnostics

Several authors have proposed numerous diagnostic approaches for planetary gearboxes, with vibration analysis the most commonly employed monitoring technology [6, 9, 15, 17, 20, 21]. However, fault detection of bearings within the planetary gearbox is one of the most challenging diagnostic scenarios, as the resulting vibration signatures are influenced by the

variable transmission paths from the bearing to the receiving externally mounted sensor. This leads to strong background noise which can mask the vibration signature of interest. This task is compounded by the fact that the gear mesh frequencies typically dominate the resultant vibration signal [15, 20, 22].

Early attempts at diagnosing defective planetary gearboxes utilized time domain averaging to separate the gear components from the measured vibration signal in order to reduce the signal-to-noise ratio (SNR). This involved combining a delayed version of the measured vibration signal with the original signal thereby reinforcing certain frequency components, whilst eliminating others. However, the signal to noise ratio (SNR) enhancement with this technique is not always sufficient to aid detection of bearing faults and hence this technique has not proved successful in identifying bearing defects within planetary gearboxes [15]. Time Synchronous Averaging (TSA) has also been applied to separate the bearing vibration components from the measured gearbox signature [20, 23, 23-26]. This minimises the influence of speed variation by re-sampling the signal in the angular domain [20]. The process of re-sampling the signal requires a tachometer or phase marker and is not commonly applied for the sole purpose of separating the bearing vibration signature [25].

Recently, signal separation techniques have been applied in the diagnosis of bearing faults within gearboxes. The separation is based on decomposing the signal into deterministic and random components. The deterministic part represents the gear component and the random part represents the bearing component of the measured signal. The bearing contribution to the signal is expected to be random due to the influence of slip experienced by the rolling elements [16, 25, 27, 28]. A number of methods for signal separation are available, each having relative advantages and disadvantages [25, 29-31]. Techniques such as Linear Prediction (LP) have been employed for separation, allowing the separation of the deterministic (or predictable) part of a signal from the random background noise using the information provided by past observations [32, 33]. The results of such techniques depend on the number of past observations considered. Smaller values of past observation produce a poor prediction, giving a negligible improvement in the signal-to-noise ratio, while very high values compromise computation time, over-constrain the prediction and tend to reduce even the

main components of the signal (both deterministic and non-deterministic parts) [34, 35]. Interestingly LP is applied only to stationary vibration signatures.

To overcome the problem of separation of non-stationary vibrations, adaptive filters were proposed. This concept is based on the Wold Theorem, in which the signal can be decomposed into deterministic and non-deterministic parts [36]. It has been applied to signal processing in telecommunication [35] and ECG signal processing [37]. The separation is based on the fact that the deterministic part has a longer correlation than the random part and therefore the autocorrelation is used to distinguish the deterministic part from the random part. However, a reference signal is required to perform the separation. The application of this theory in condition monitoring was established by Chaturvedi et al. [38] where the Adaptive Noise Cancellation (ANC) algorithm was applied to separate bearing vibrations corrupted by engine noise, with the bearing vibration signature used as a reference signal for the separation process. However, for practical diagnostics, the reference signal is not always readily available. As an alternative, a delayed version of the signal has been proposed as a reference signal and this method is known as self-adaptive noise cancellation (SANC) [28] which is based on delaying the signal until the noise correlation is diminished and only the deterministic part is correlated [27].

Many recursive algorithms have been developed specifically for adaptive filters [39, 40]. Each algorithm offers its own features and therefore, the algorithm to be employed should be selected carefully depending on the signal under consideration. Selection of the appropriate algorithm is determined by many factors, including convergence, type of signal (stationary or non-stationary) and accuracy [41].

More recently Spectral Kurtosis (SK) technique has been introduced for bearing signal separation [42]. The basic principle of this method is to determine the Kurtosis at different frequency bands in order to identify the energy distribution of the signal and determine where the high impact energy (transient events) are located in the frequency domain. Obviously, the results obtained strongly depend on the width of the frequency bands (Δf) [43]. As noted earlier, in real applications background noise often masks the signal of interest and, as a result, the traditionally obtained Kurtosis value, in the time domain, is unable to capture the ‘peakiness’

of the fault signal, usually giving low Kurtosis values. Therefore, in applications with strong background noise, the Kurtosis as a global indicator is not useful, although it gives better results when it is applied locally in different frequency bands [42]. The Spectral Kurtosis (SK) was first introduced by Dwyer [44] as a statistical tool which can locate non-Gaussian components in the frequency domain of a signal. This method is able to indicate the presence of transients in the signal and show their locations in the frequency domain. It has been demonstrated to be effective even in the presence of strong additive noise [42, 45].

In addition to vibration analysis, the use of Acoustics Emissions (AE) technology has emerged as a promising diagnostic approach. AE was originally developed for non-destructive testing of static structures, however, in recent times, its application has been extended to health monitoring of rotating machines and bearings [46-49]. In machinery monitoring applications, AE are defined as transient elastic waves produced by the interface of two components or more in relative motion [50, 51]. AE sources include impacting, cyclic fatigue, friction, turbulence, material loss, cavitation, leakage, etc. It provides the benefit of early fault detection in comparison to vibration analysis and oil analysis due to the high sensitivity to friction offered by AE [52]. Nevertheless, successful applications of AE for health monitoring of a wide range of rotating machinery have been partly limited due to the difficulty in signal processing, interpreting and manipulating the acquired data [53-55]. In addition, AE signal processing is challenged by the attenuation of the signal and as such the AE sensor has to be close to its source. However, it is often only practical to place the AE sensor on the non-rotating member of the machine, such as the bearing housing or gearbox casing. Therefore, the AE signal originating from the defective component will suffer severe attenuation and reflections, before reaching the sensor. Challenges and opportunities of applying AE to machine monitoring have been discussed by Sikorska et. al and Mba et. al. [51, 56]. To date, most applications of machine health monitoring with AE have targeted single components such as a pair of meshing gears [57], a particular bearing or valve [58, 59]. This targeted approach to application of AE has on the whole demonstrated success. However the ability to monitor components that are secondary to the main component of interest such as a bearing supporting a gear, as is the case with planetary gears in an epicyclical gearbox, has not been well-explored. This is the first known publication to explore the ability to identify a fault condition where the AE signature of interest is severely masked by the presence of gear

meshing AE noise. Also notably, it is the first known application on a commercial helicopter main gearbox.

Whilst vibration analysis of gearbox fault diagnosis is well established, the application of AE to this field is still in its early stages [52, 60, 61]. Moreover, there are limited publications on application of AE to bearing fault diagnosis within gearboxes [54]. This paper discusses the analysis of vibration and AE data collected from a CS-29 category 'A' helicopters industrial test facility and compares their effectiveness in diagnosing a bearing defect in the epicyclic module of helicopter main gearbox. This paper focuses on the new AE sensing technologies available for fault detection, with a particular emphasis on increasing the signal separation of the " defect signal". The data was collected for various bearing fault conditions and processed using an adaptive filter algorithm to separate the non-deterministic part of the signal and enhance the signal-to-noise ratio for both AE and vibration. The resultant signatures were then further processed using envelope analysis to extract the fault signature.

3 Gear and bearing diagnostics

The vibration signals associated with bearing defects have been extensively studied and robust detection algorithms are now available as off-the-shelf solutions [62]. Conversely, the dynamics associated with bearing diagnostics within gearboxes reduce the effectiveness of traditional techniques. Therefore, it is important to understand the nature of the faulty bearing signal.

For rolling element bearings, a fault will cause shocks which in turn excite higher resonance frequencies which will be amplitude modulated depending on two factors, the transmission path and loading condition [26]. Therefore, the vibration signal is typically demodulated to extract the frequency of these impulses. Equations for calculation of bearing faults frequencies have been reported widely in the literature [20, 63, 64]. These equations assume no slip, however, in operation there is some degree of slip and this why the bearing faults frequencies vary by 1% to 2% of the calculated value. It is this slip that facilitates the separation of the gear and bearing vibration components [16], the latter known as the non-deterministic component of the measured vibration. The deterministic part of the signal is

usually related to gear and shaft speeds [21]. Such periodic events are related to kinematic forces induced by the rotating parts such as meshing forces, misalignment and eccentricity [29]. In some cases the deterministic part of the vibration signal cannot be identified due to speed variation, and therefore, it essential to re-sample the signal to the angular domain in order to track speed variation [29, 65]. The deterministic part of the signal can be used for diagnostics of gear and shaft faults.

In relation to AE only relatively short time series signatures are typically processed [60]. In application to diagnosis of machine faults, simple AE parameters are typically employed, such as rms, kurtosis, AE counts [51] and demodulation [46]. More recently the use of Spectral Kurtosis and adaptive filters has been employed to facilitate the diagnosis of machine faults with AE [47-49].

4 Signal processing and data analysis

Bearing and gear fault identification involves the use of various signal processing algorithms to extract useful diagnostic information from measured vibration or AE signals. Traditionally, analysis has been grouped into three classes; time domain, frequency domain, and time-frequency domain. The statistical analysis techniques are commonly applied for time domain signal analysis, in which descriptive statistics such as rms, skewness, and kurtosis are used to detect the faults [66, 67]. A fast Fourier transform (FFT) is commonly used to obtain the frequency spectra of the signals. The detection of faults in the frequency domain is based on the identification of certain frequencies which are known to be typical symptoms associated with bearing or gear faults. The time-frequency domain methods are composed of the short-time Fourier transform (STFT) [68], Wigner-Ville [66], and wavelet analysis [69, 70]. The use of these detection techniques are feasible for applications where a single component is being monitored however for applications that include several components, such as gearboxes, it is essential to employ separation algorithms. For this study, the vibration and AE signals acquired were processed by firstly employing an adaptive filter algorithm to estimate the deterministic component of the signal. Secondly, spectral kurtosis was used to estimate the filter characteristics of the deterministic signal for envelope analysis.

Lastly, a frequency spectrum of the enveloped signal was determined. The signal processing procedures are summarised in Figure 1, with descriptions detailed in the following section.

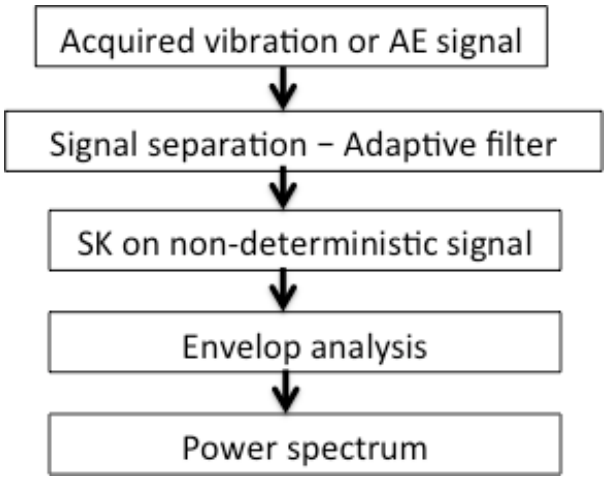

Figure 1 Signal processing algorithms flow chart

An adaptive filter [41, 45, 71] is used to model the relationship between two signals in an iterative manner; the adaption refers to the method used to iterate the filter coefficient. The adaptive filter solution is not unique; however the best solution is that which is closest to the desirable response signal [72]. FIR filters are more commonly used as adaptive filters in comparison to IRR filters [73]. The adaptive filter principle is based on Wold theorem which proposes that the vibration signal can be decomposed into two parts, deterministic and random [40, 72-74] .The random signal then processed using envelope analysis, Envelope analysis is applied extensively in vibration analysis for the diagnosis of bearings and gearboxes [17, 22, 22, 22, 26, 26, 26]. As impacts due to the defects excite resonance at higher frequencies, it is possible to identify the frequency of the impacts with the use of envelope analysis. In application, the vibration signal is filtered at high frequencies (structural resonance frequencies) and then the signal is passed through an envelope detector and a low pass filter. The enveloped signal is either presented in the time domain or transformed into the frequency domain in order to identify fault frequency components [75]. In order to detect fault signatures, it is important to select filter parameters carefully. In addition, Spectral Kurtosis (SK) has been applied to select such filter parameters [42, 76]. The basic principle of the SK method is to determine the Kurtosis at different frequency bands in order to identify the energy distribution of the signal and to determine where the high impact (transient) energy is located in the frequency domain.

The results obtained are strongly dependent on the width of the frequency bands Δf [43]. The Kurtogram [32] is a representation of the calculated values of the SK as a function of f and Δf. However, exploration of the entire plane (f, Δf) is a complicated computational task, though Antoni [43] suggested a methodology for the fast computation of the SK.

5 Experimental Setup

Experimental data was obtained from tests performed on CS-29 Category 'A' helicopter gearbox which was seeded with defects in one of the planetary gears bearing of the second epicyclic stage. The test rig was of back-to-back rig configured and powered by two motors simulating dual power input.

5.1 CS-29 'Category A' helicopter main gearbox

The transmission system of a CS-29 'Category A' helicopter gearbox is connected to two shafts, one from each of the two free turbines engines, which drive the main and tail rotors through the MGB. The input speed to the MGB is typically in the order of 23,000 rpm, which is reduced to the nominal main rotor speed of 265 rpm, see figure 2.

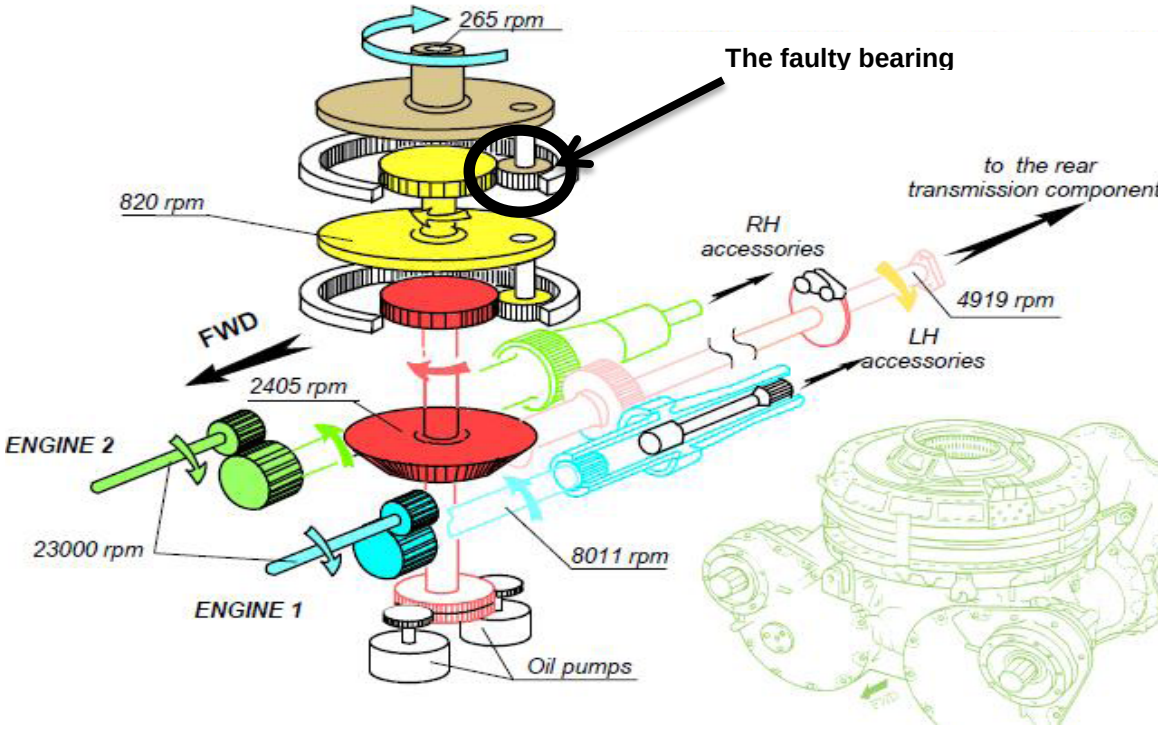

Figure 2 Gearbox internal parts [19]

The main rotor gearbox consists of two sections, the main module, which reduces the input shaft speed from 23,000 rpm to around 2,400 rpm. This section includes two parallel gear stages. This combined drive provides power to the tail rotor drive shaft and the bevel gear. The bevel gear reduces the rotational speed of the input drive to 2,405 rpm and changes the direction of the transmission to drive the epicyclic reduction gearbox module. The second section is the epicyclic reduction gearbox module which is located on top of the main module. This reduces the rotational speed to 265 rpm which drives the main rotor. This module consists of two epicyclic gears stage, the first stage contains 8 planets gears and second stage with 9 planets gears, see figure 3. The details of the gears are summarised in table 1.

Figure 3 Second stage epicyclic gears

Table 1 number of teeth for the gearbox gears

First parallel stage	Pinion teeth	Wheel teeth	
	23	66	
Second parallel stage	Pinion teeth	Wheel teeth	
	35	57	
Bevel stage	Pinion teeth	Bevel teeth	
	22	45	
1st epicyclic stage	Sun gear	Planets gear – 8 gears	Ring gear
	62	34	130
2nd epicyclic stage	Sun gear	Planets gear – 9 gears	Ring gear
	68	31	130

The epicyclic module planet gears are designed as a complete gear and bearing assembly. The outer race of the bearing and the gear wheel are a single component, with the bearing rollers running directly on the inner circumference of the gear. Each planet gear is 'self-aligning' by the use of spherical inner and outer races and barrel shaped bearing rollers (see Figure 3).

5.2 Experimental conditions and setup

This investigation involved performing the tests for the fault-free condition, minor bearing damage and major bearing damage. The bearing faults were seeded on one of the planet gears of the second epicyclic stage. Minor damage was simulated by machining a rectangular section of fixed depth and width across the bearing outer race (10mm wide and 0.3mm deep), see figure 4, and the major damage simulated as a combination of both a damaged inner race (natural spalling around half of the circumference) and an outer race (about 30mm wide, 0.3mm deep), see figure 5. Three load conditions were considered for the each fault condition, 110% of maximum take-off power, 100% and 80% of maximum continuous power; the power, speed and torque characteristics of these load conditions are summarised in table 2.

Figure 4 Damaged slot across the bearing outer race

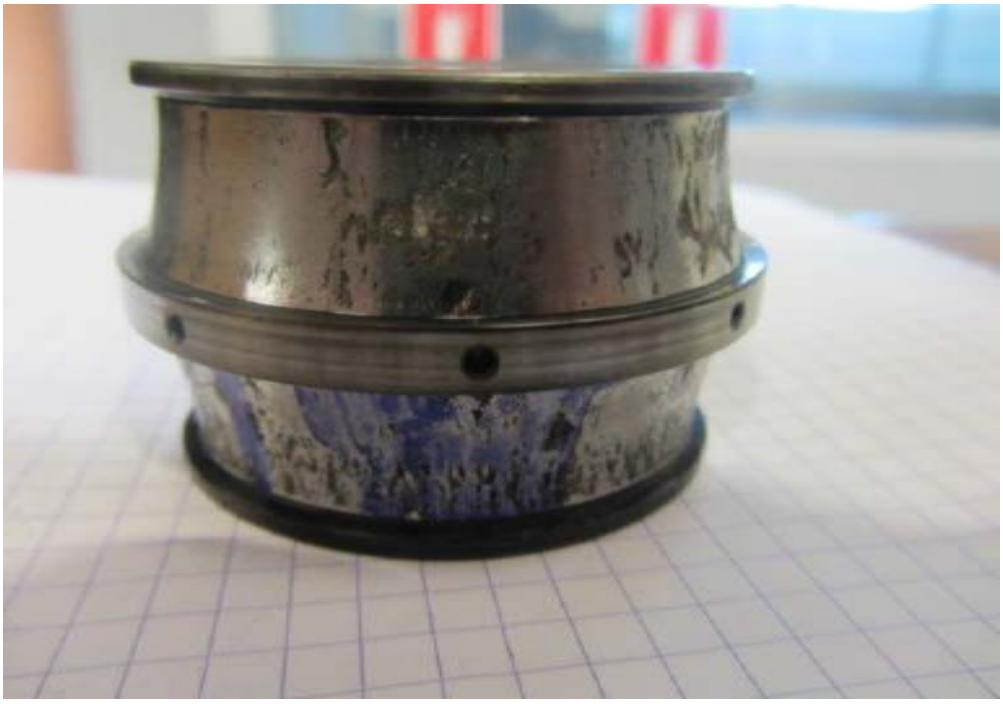

Figure 5 Inner race natural spalling

Table 2 Test Load conditions characteristics

Load Condition	Power (Kw)	Rotor speed (RPM)	Right input torque (Nm)	Left input torque Nm)
110% Max take-off power	1760	265	368	368
100% Max continuous power	1300	265	272	272
80% Max continuous power	936	265	196	196

5.3 Vibration fault frequencies

To aid diagnosis, all characteristic vibration frequencies were determined, see table 3. These included gears mesh frequencies of the different stages and the bearing defect frequencies for planet bearing.

Table 3 Gearbox characteristic frequencies

Frequency components	Frequency HZ
Gears Meshes	
First parallel GMF Hz	8751.5
Second parallel GMF	4640.94697
Bevel stage GMF (Hz)	1791.24269
1st epicyclic stage GMF	1671
2nd epicyclic stage GMF	573
Faulty planet bearing	
Ball spin	45.31426
Outer race	96.69819
Inner race	143.9603
Cage	7.438322

5.4 Data acquisition and instrumentation

Vibration data was acquired with a triaxial accelerometer (type PCB Piezotronics 356A03) at a sampling frequency of the 51.2 kHz. The accelerometer had an operating frequency range of 2 Hz to 8 kHz and was bonded to the case of the gearbox, see figure 6. The acquisition system employed was a National Instruments (NI) NI cDAQ-9188XT Compact DAQ Chassis. A 60 second sample was recorded for each fault case. The Y-axis of the tri-axial accelerometer arrangement was oriented parallel to the radial direction of the gearbox, the X-axis to the tangential axis, and the Z-axis is the vertical axis parallel to the rotor axis, see figure 6.

In addition, Acoustic Emission data was collected using a PWAS sensor [77], 7mm diameter and approximately 0.2mm thick, bonded to the upper face of the planet carrier, see figure 7. The sensor was connected to a conditioning board, attached to the planetary carrier, prior to wirelessly transmission, see figure 7. The wireless transfer was accomplished by utilising two single turn brass coils of approximately 400 mm diameter, which were cut to size using water jets for accuracy. One

coil was fixed and the other rotating coil moved with the component being investigated, upon which is mounted a sensor. The sensor-side circuitry is required to be very small and must be self-powered without the use of a battery. To achieve this, the system makes use of Radio Frequency (RF) power-scavenging. The system uses a homodyne receiver with a "modulated backscatter" communications link, to pass the analogue signal across the wireless link. The stationary (upper) coil was suspended from two clamping rings that were attached to the top case of the gearbox with a spacer through the holes to retain location. The moving (lower) coil was attached to a circular mounting ring which was, in turn, mounted on top of the oil caps on the planet carrier, see figures 8 and 9. Electrical isolation of the coils from the mounts and surrounding metallic structure was achieved through the use of nylon washers and bushes. AE data was acquired at a sampling rate of 5 MHz using an NI PCI-6115 card connected to a BNC-2110 connector block.

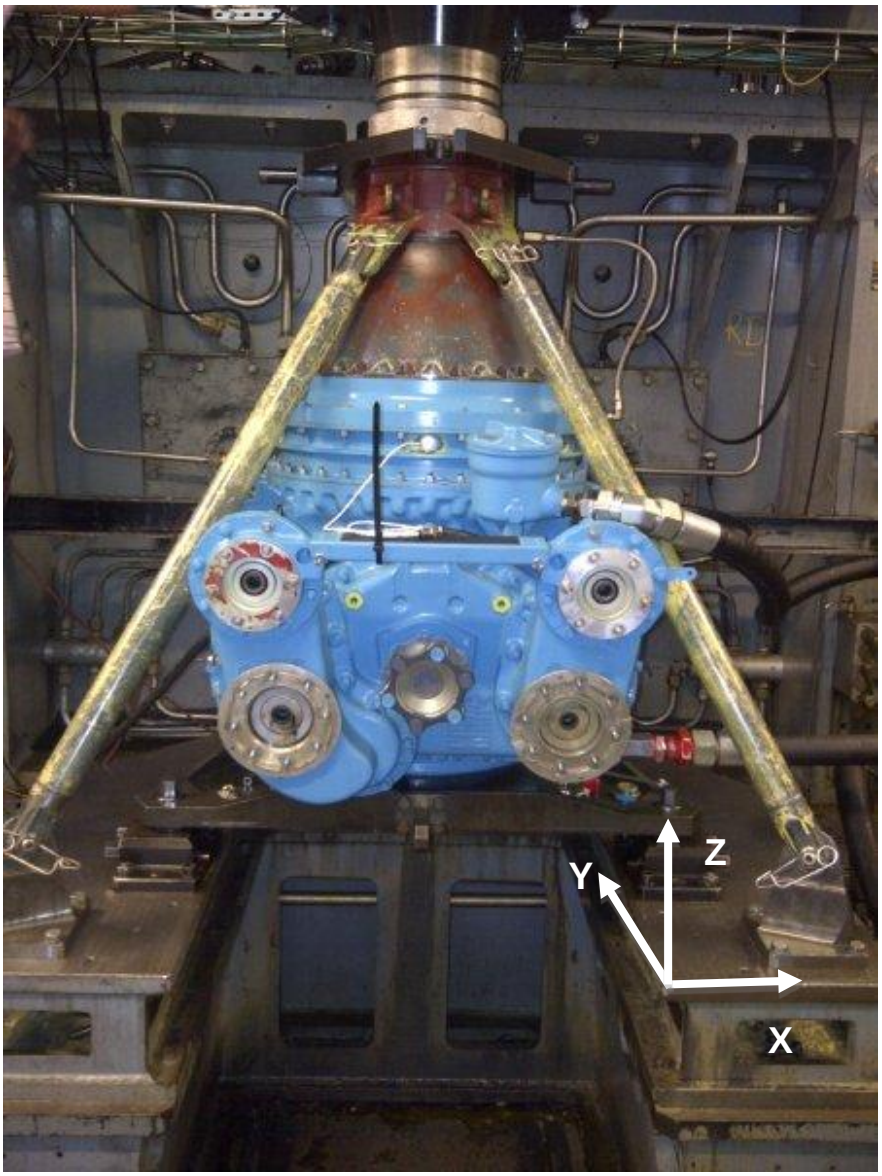

Figure 6 MGB installed on the test bench

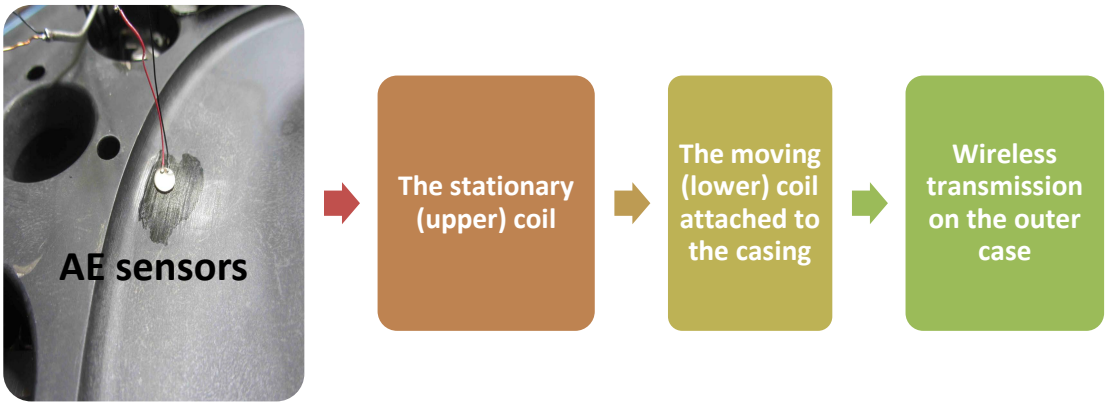

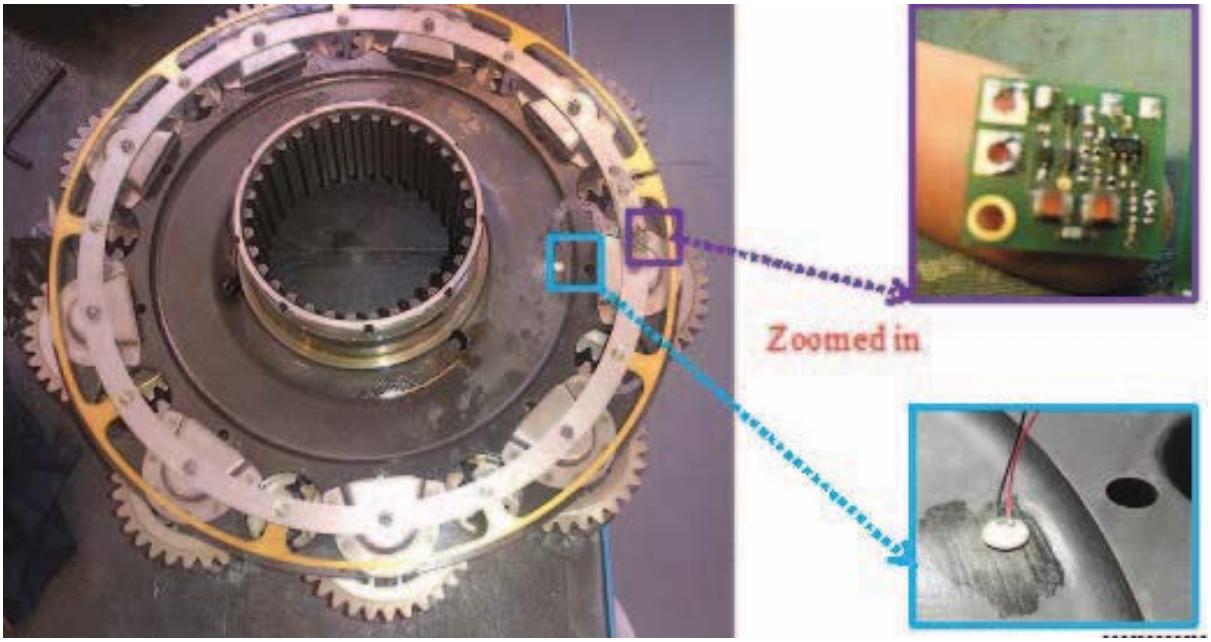

Figure 7 AE Wireless transmission scheme

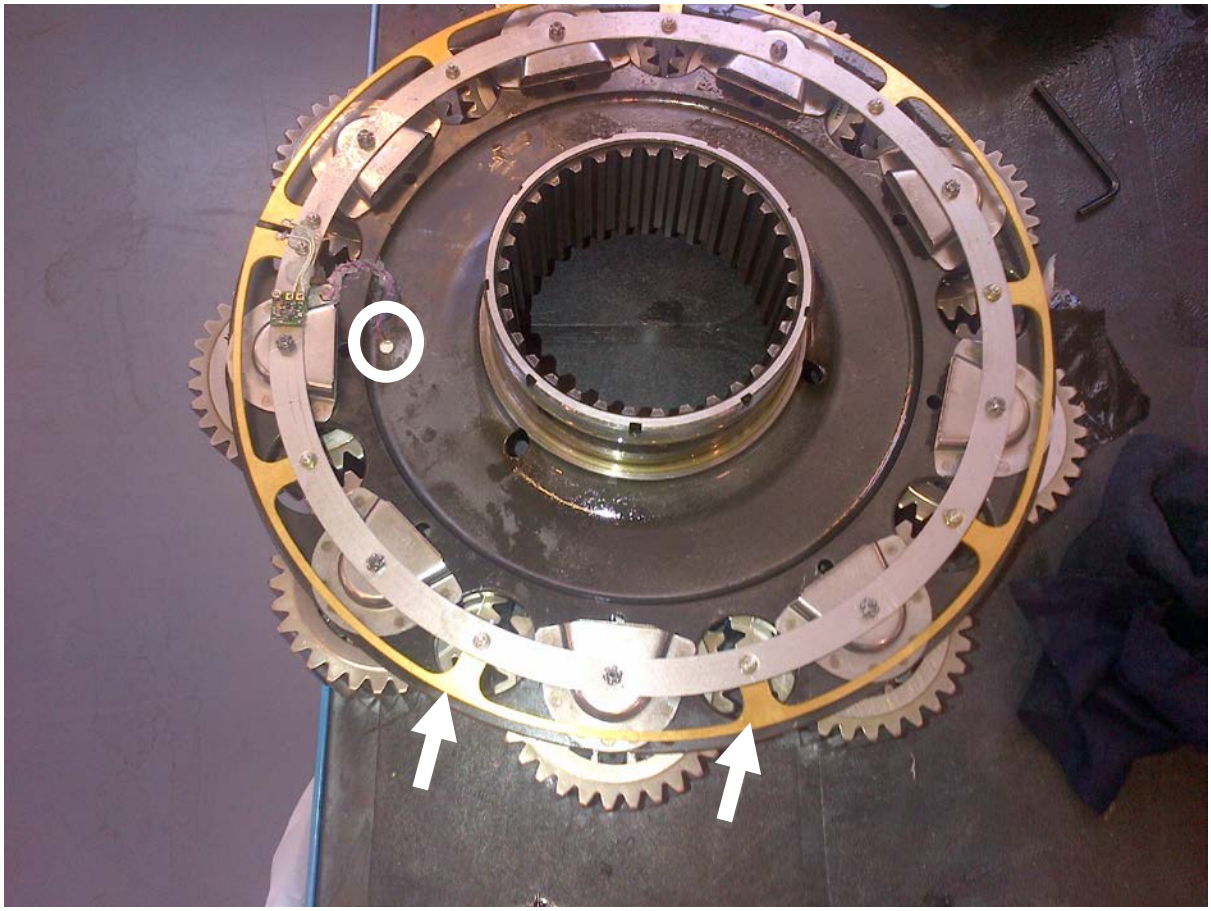

Figure 8 Moving coil mounted on the planetary carrier (coil arrowed, sensor circled)

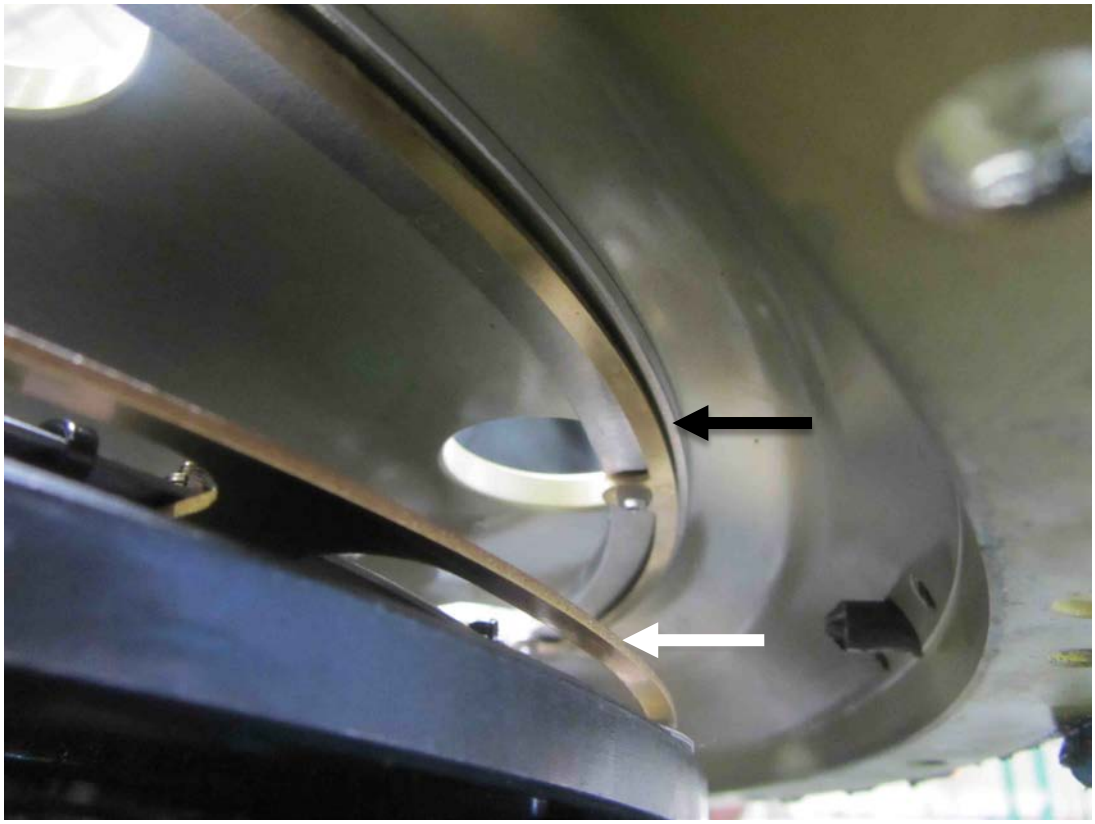

Figure 9 Coils in position prior to assembly (static coil black arrow, moving coil white arrow)

6 Observations of vibration analysis

The measured vibration data was processed to estimate the power spectrum of the vibration signal for damaged conditions, see figure 10. This analysis was performed to assess the ability of FFT spectrum to determine the fault signature. The results show clearly that no distinctive planetary bearing fault frequency was evident in the spectrum, and it was observed that the gear mesh frequencies (GMFs) dominate the spectrum. Therefore, the data was further processed using signal separation and Spectral Kurtosis to identify the fault signature as described earlier.

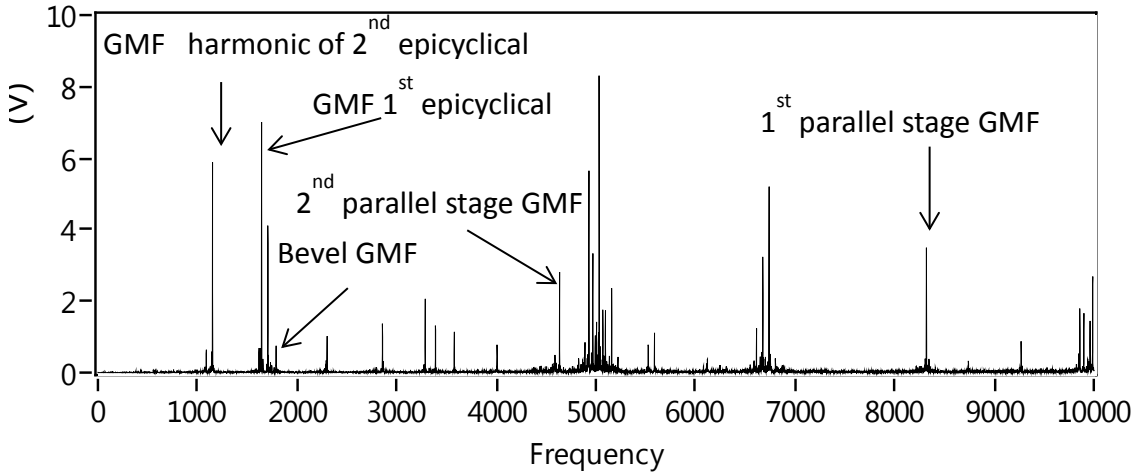

Figure 10 Power spectrum of original vibration signal for the major defect condition

In order to ensure the optimal LMS algorithm parameter estimation; the Mean Square Error (MSE) was determined, figure 11 shows the MSE converge to the minimum. Figure 12(a) and (b) shows the vibration signature prior and after to signal separation of the deterministic components for the small defect test condition. This result shows the non-deterministic component of the signal following separation, highlighting the fact that no periodic impact shocks were evident for the small defect condition; this observation also applied to the large defect condition.

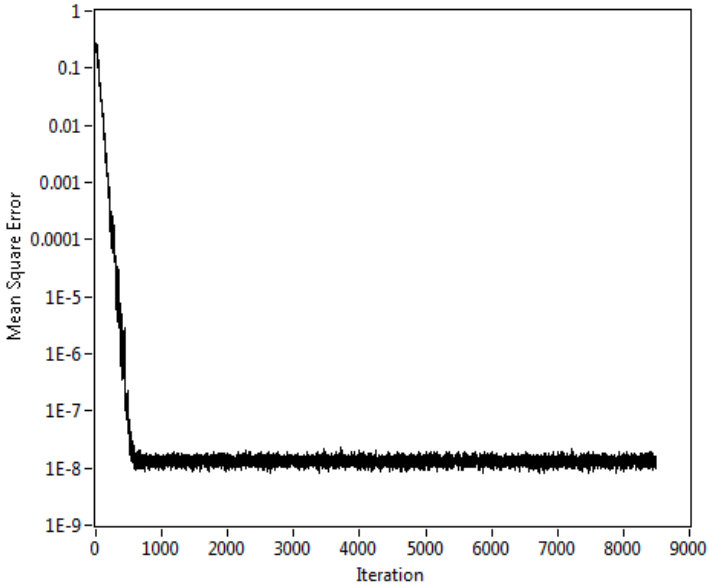

Figure 11 LMS convergence

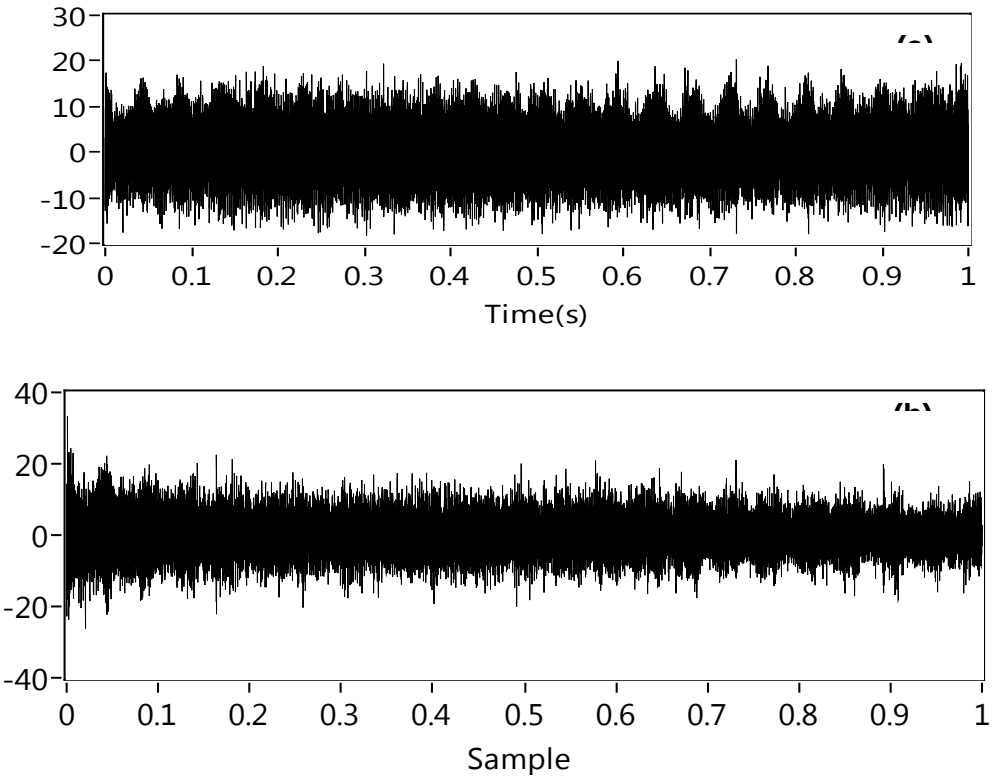

Figure 12 Time waveform of vibration signatures (a) before and (b) after separation for small defect

Spectral Kurtosis analysis was undertaken on the non-deterministic part of data sets collected from the gearbox for the different fault cases and this yielded the frequency bands and center frequencies which were then used to undertake envelope analysis. As discussed earlier the signal separation was undertaken with an adaptive filter LMS algorithm.

Observation from a typical Kurtogram used to estimate the associated filter characteristics for different defect conditions is shown in figure with corresponding filter frequency bands at 110% maximum take-off power summarised in table 4. The SK results show there was a significant increase of maximum kurtosis for major damaged compared to fault-free and minor damage condition, typically 500-600% higher in all measurement directions, see table 4. However, no significant differences were identified between minor and fault-free conditions. Spectral plots of enveloped vibration signals following filtration, whose characteristics were determined with the aid of the kurtogram, are shown in figures 16 to 26.

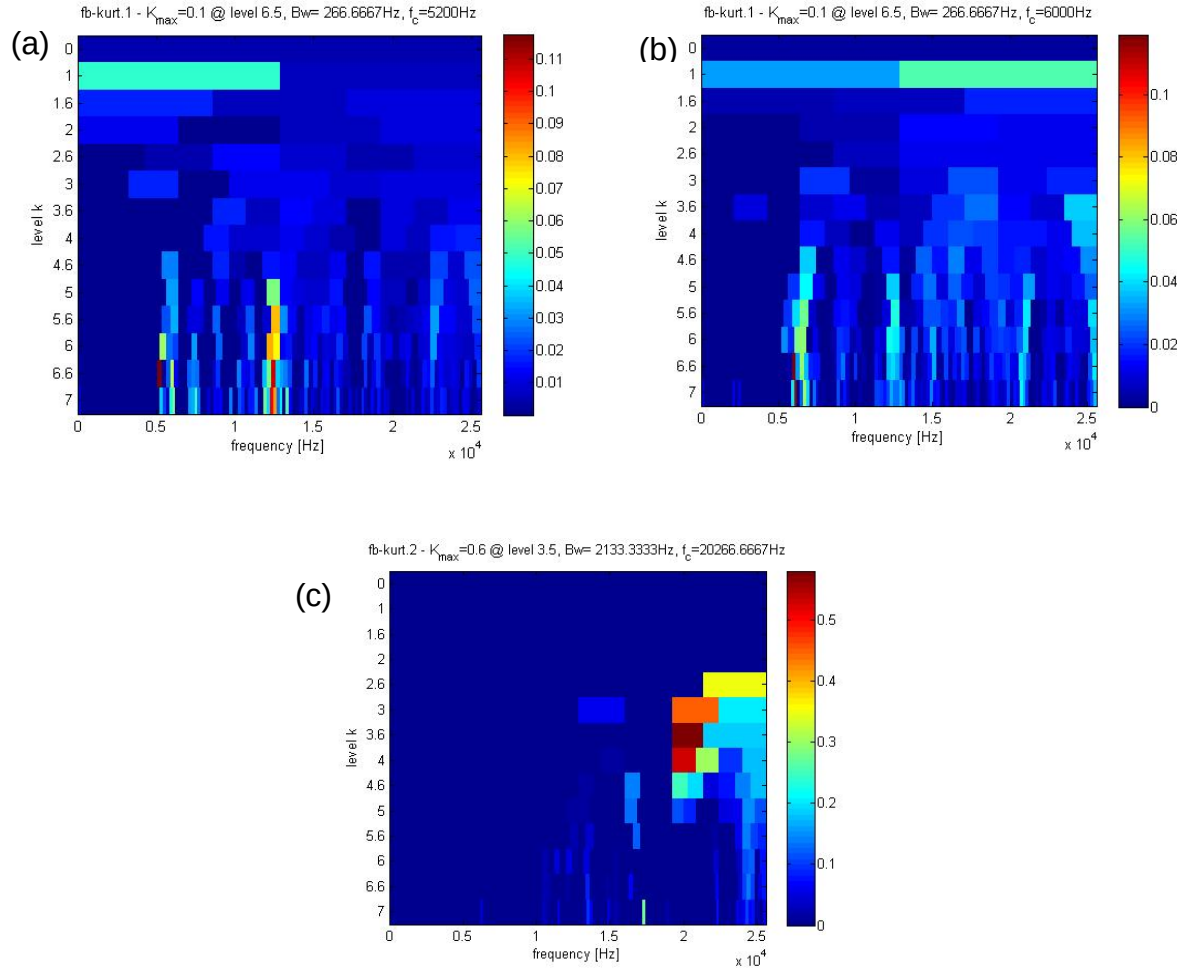

Figure 13 Kurtograms of non-deterministic signal for (a) Fault-free (b) Minor damage (c) Major damage (110% maximum take-off power, X direction)

Table 4 Filter characteristics estimated based on SK for all three vibration axes at 110% maximum take-off power

Case	Center frequency F_c (Hz)	Band Width Bw (Hz)	Kurtosis
Fault-free condition X direction	5200	266	0.1
Fault-free condition Y direction	5200	266	0.1
Fault-free condition Z direction	5200	266	0.11
Minor damage condition X direction	6000	266	0.11
Minor damage condition Y direction	6000	266	0.1
Minor damage condition Z direction	6000	266	0.12
Major damage condition X direction	20266	2133	0.5
Major damage condition Y direction	20266	2133	0.45
Major damage condition Z direction	20266	2133	0.6

Observation from the spectra of the enveloped signal in the X direction at 110% maximum take-off power, 100% and 80% maximum continuous power, see figures 13, 14 and 15 respectively, showed no presence of fault frequencies associated with the defective planetary bearing in the spectrum, except for the case of 110% maximum take-off power, see figure 13, where the outer race defect frequency (96 Hz) and the 2nd harmonic of cage defect frequency (15 Hz) were detected. However, the minor fault condition was not identified. It is apparent that the signal separation had not completely removed the gear mesh and shaft frequencies, particularly the sun gears frequencies and its harmonics for first and second epicyclic stages (38.8 and 13.2 Hz respectively), which were detected, see figures 13, 14 and 15. The existence of these frequencies is due to the fact that the vibration signal used in this analysis wasn't synchronised to any particular shaft.

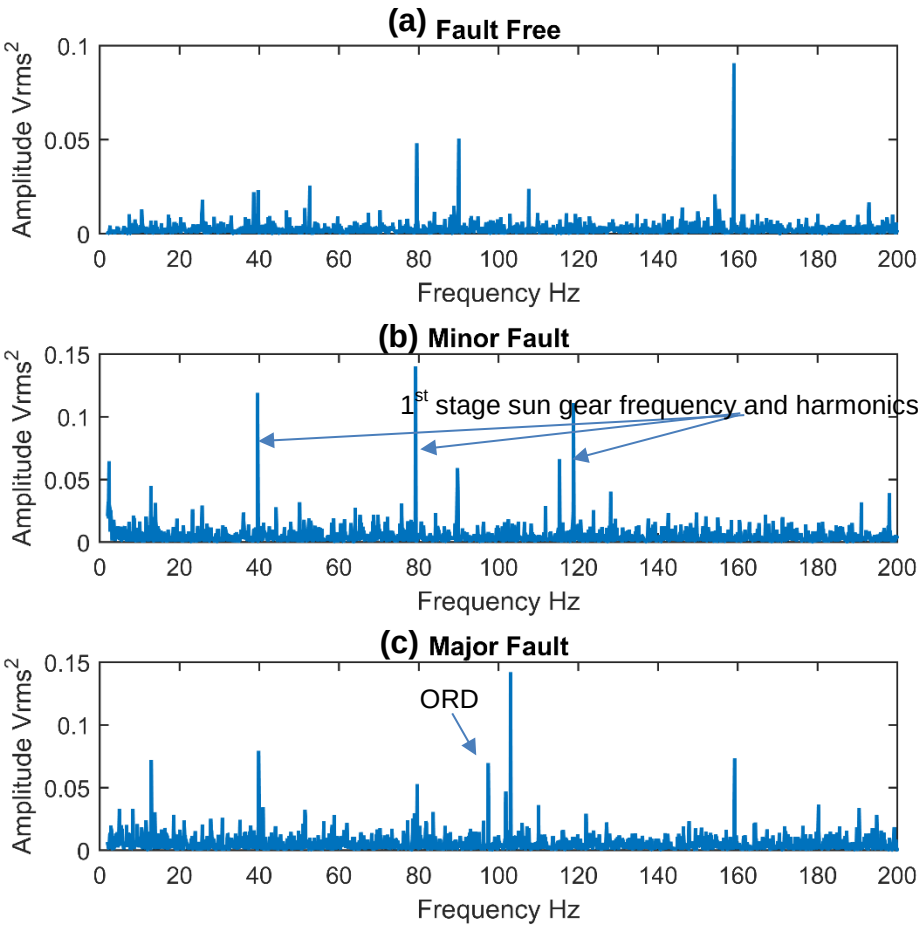

Figure 13 Enveloped Spectra of non-deterministic signal for (a) Fault-free (b) Minor (c) Major damage (110% of maximum take-off power, X direction)

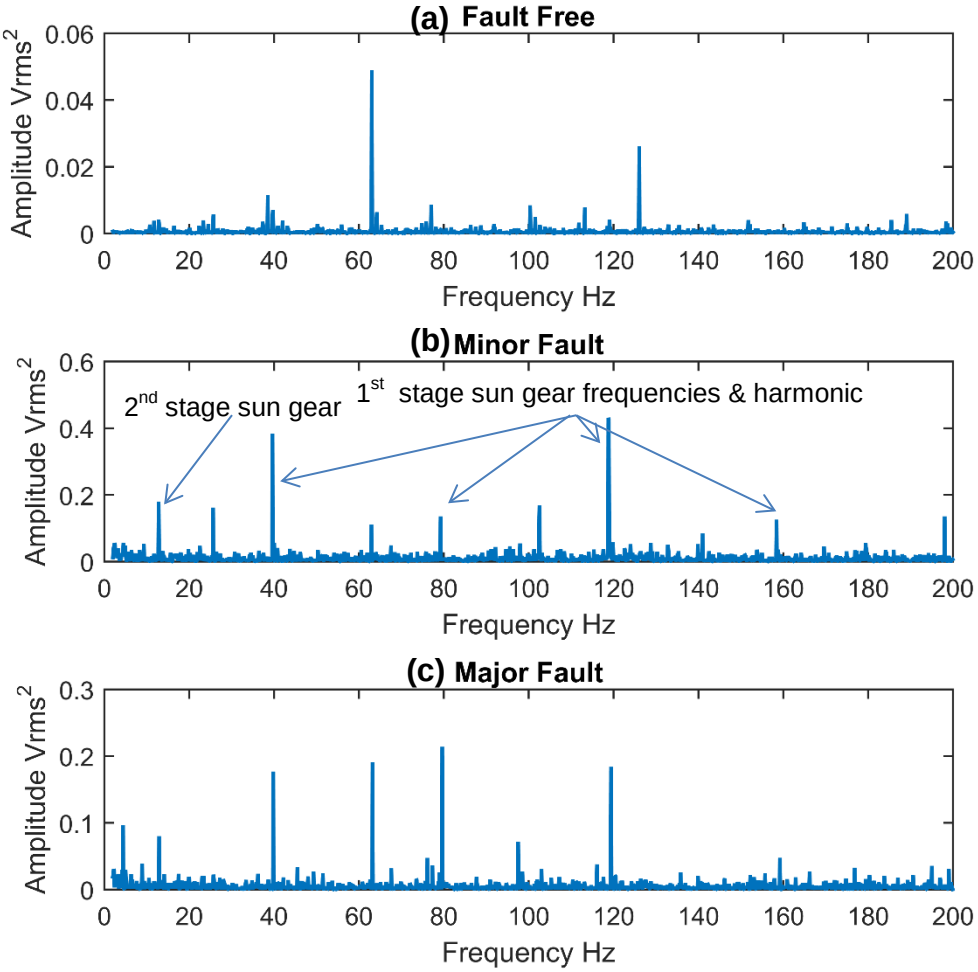

Figure 14 Enveloped Spectra of the non-deterministic signal for a) Fault-free (b) Minor (c) Major damage (100% maximum continuous power, X direction).

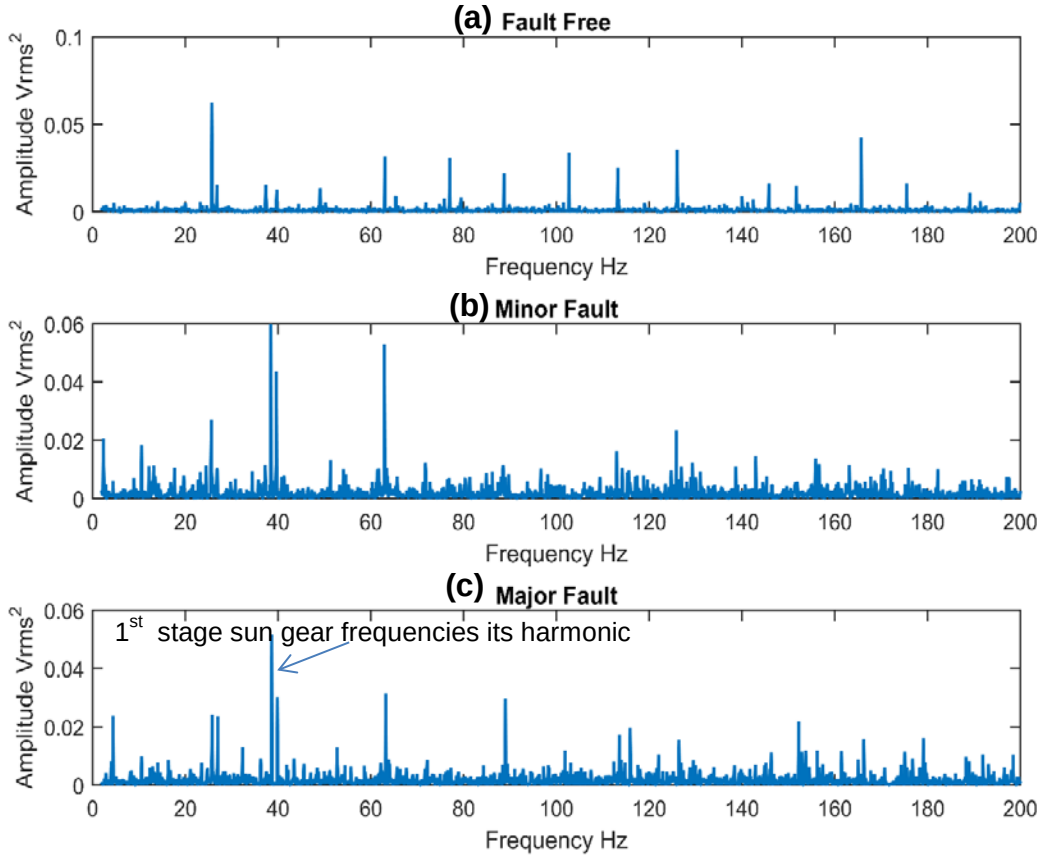

Figure 15 Enveloped Spectra of the non-deterministic signal for a) Fault-free (b) Major (c) Minor damage (80% of maximum continuous power, X direction).

Results of Y direction, see figures 16, 17 and 18 , showed the presence of the outer race defect frequency (96 Hz) for both minor and major fault cases at 110% of maximum take-off power, whilst no fault frequency was identified in envelope spectra for the 100% and 80% maximum continuous power, reinforcing the observations noted from measurements taken in the X direction. Furthermore, sun and planet gears frequencies were observed in the envelope spectrum for the measurement in this direction (Y-direction).

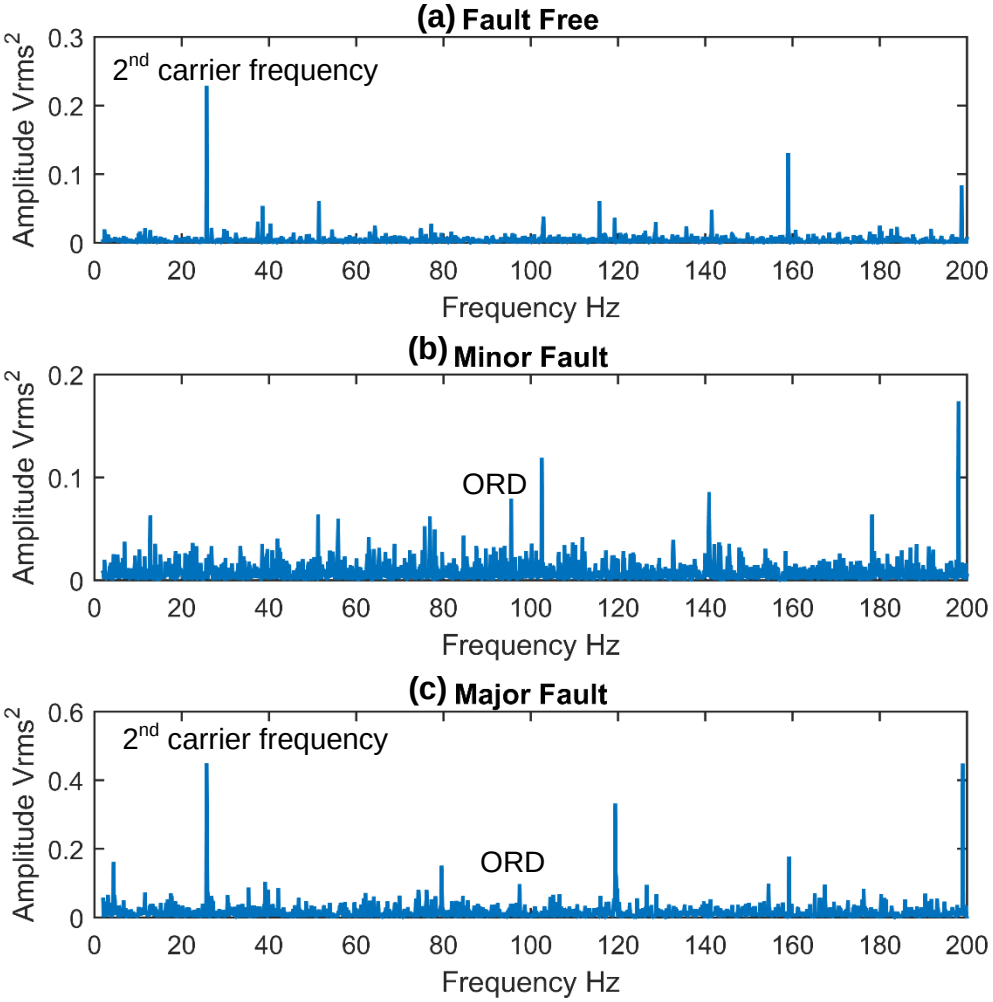

Figure 16 **Enveloped Spectra of non-deterministic signal for a) Fault-free (b) Minor (c) Major damage (110% of maximum take-off power, Y direction).**

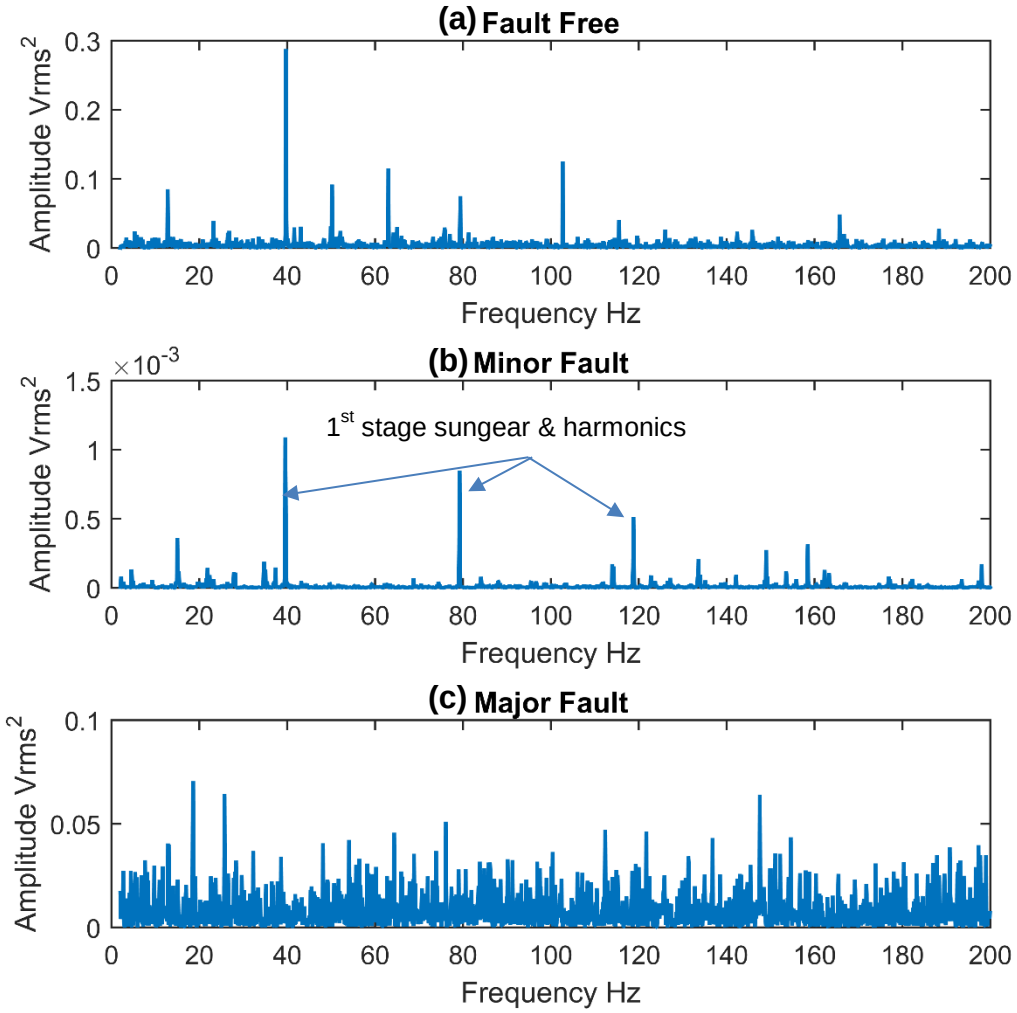

Figure 17 **Enveloped Spectra of the non-deterministic signal for a) Fault-free (b) Minor (c) Major damage (100% of maximum continuous power, Y direction).**

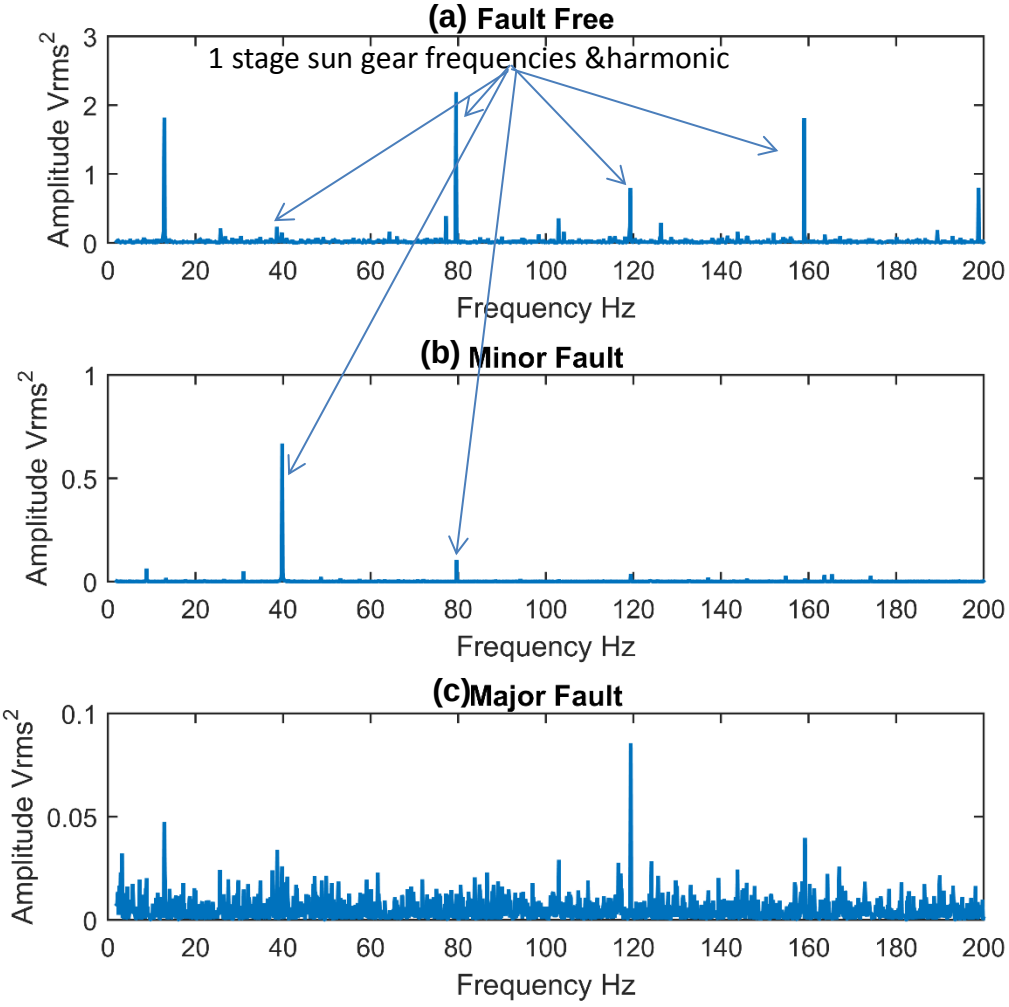

Figure 18 **Enveloped Spectra of the non-deterministic signal for (a) Fault-free (b) Minor (c) Major damage. (80% of maximum continuous power, Y direction).**

Observations of measurements taken in the Z direction, see figures 19, 20 and 21 showed the presence of the outer race defect frequency (96 Hz) and its harmonic at 110%maximum take-off power for both minor and major fault cases, reinforcing the observations in the Y direction The cage fault frequency was identified in envelope spectra for the major defect at 100% maximum continuous power and minor defect condition at 80% maximum continuous power. Compared to X and Y directions the observations in the Z direction showed the presence of some gears frequencies in envelope spectra such as first stage sun gear frequency (38.8 Hz) and it harmonics.

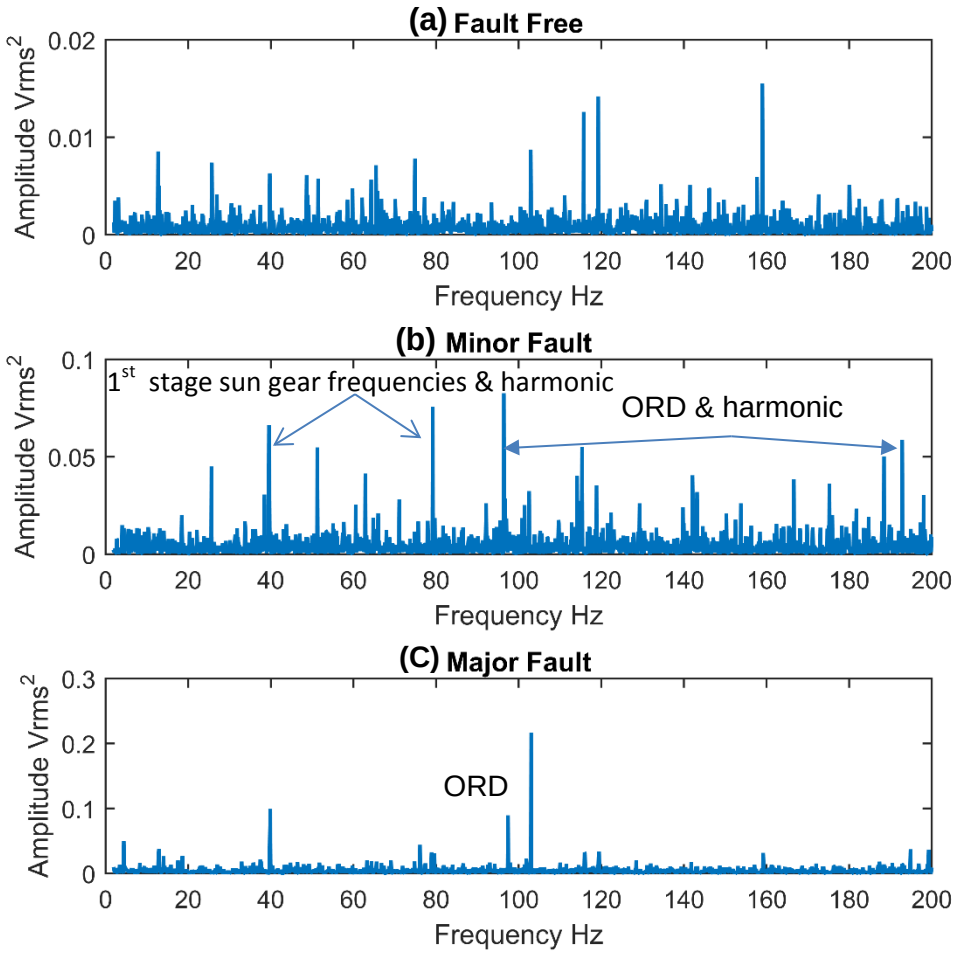

Figure 19 **Enveloped Spectra of the non-deterministic signal for a) Fault-free (b) Major (c) Minor damage (110% of maximum take-off power, Z direction).**

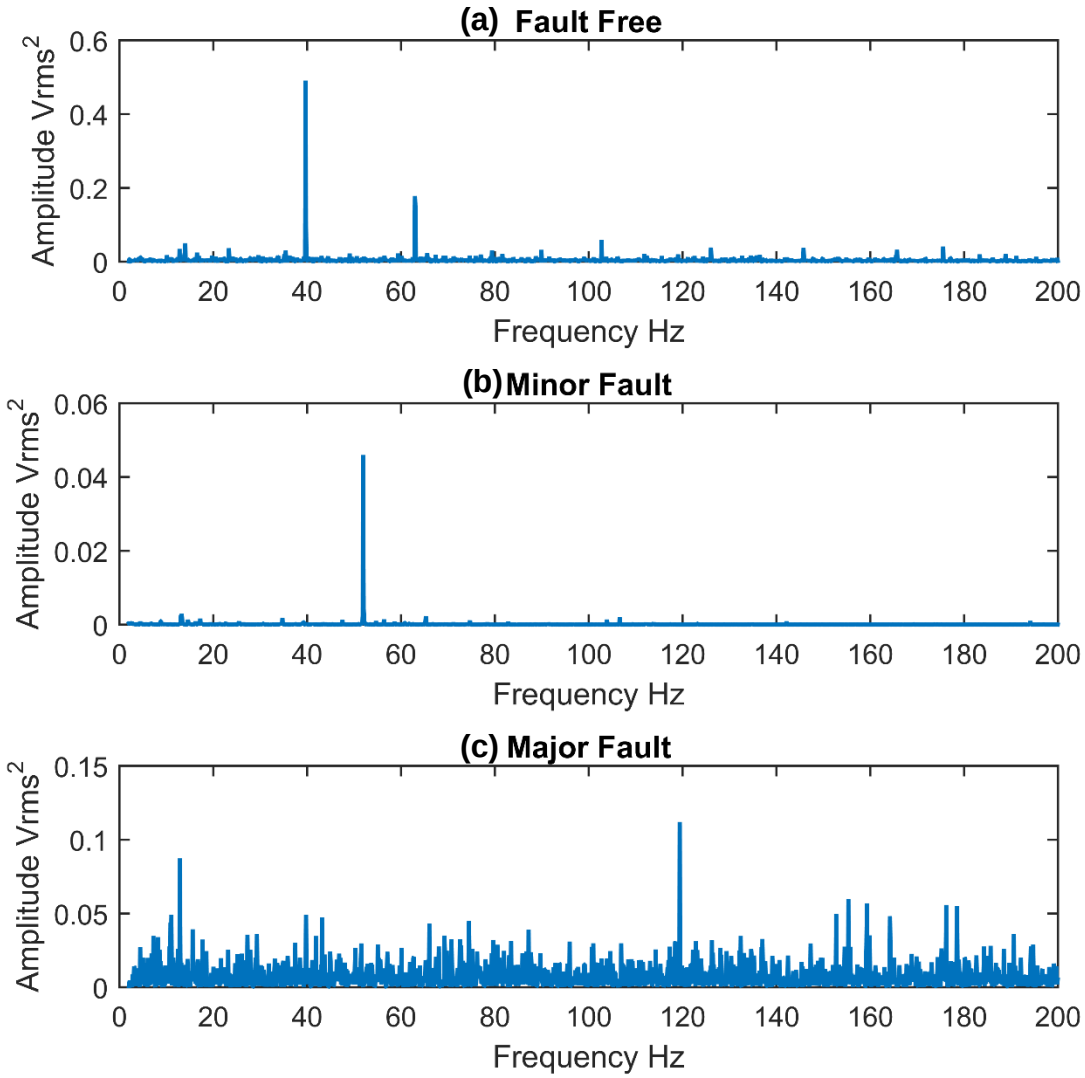

Figure 20 **Enveloped Spectra of the non-deterministic signal for a) Fault-free (b) Minor (c) Major damage (100% of maximum continuous power, Z direction)**

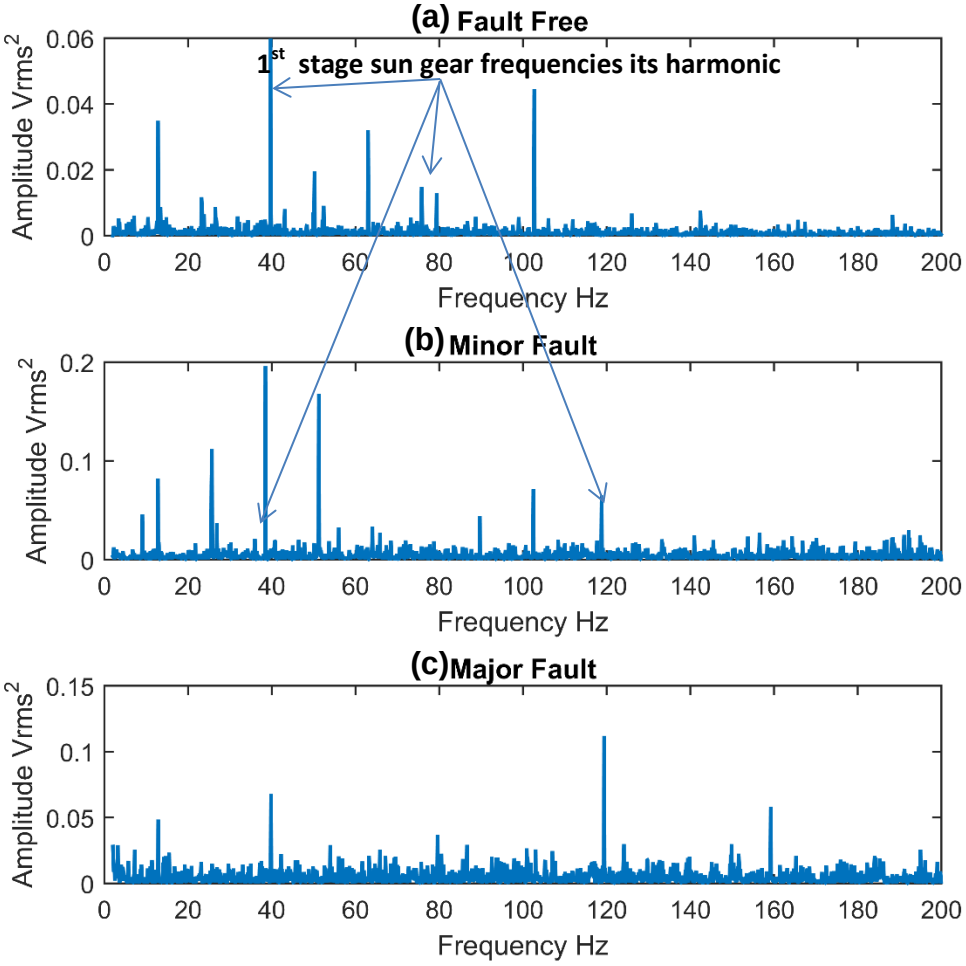

Figure 21 Enveloped Spectra of the non-deterministic signal for a) Fault-free (b) Minor (c) Major damage (80% of maximum continuous power, Z direction).

7 Acoustic Emission observations

A typical AE waveform associated with 100% maximum continuous power is presented in figure 22. Noted was the intermittent breakup of the AE signal, as highlighted in figure 22. The frequency of the signal loss corresponded to the second epicyclic stage gear mesh frequency. Irrespective of this signal breakage further processing was undertaken on the acquired waveform.

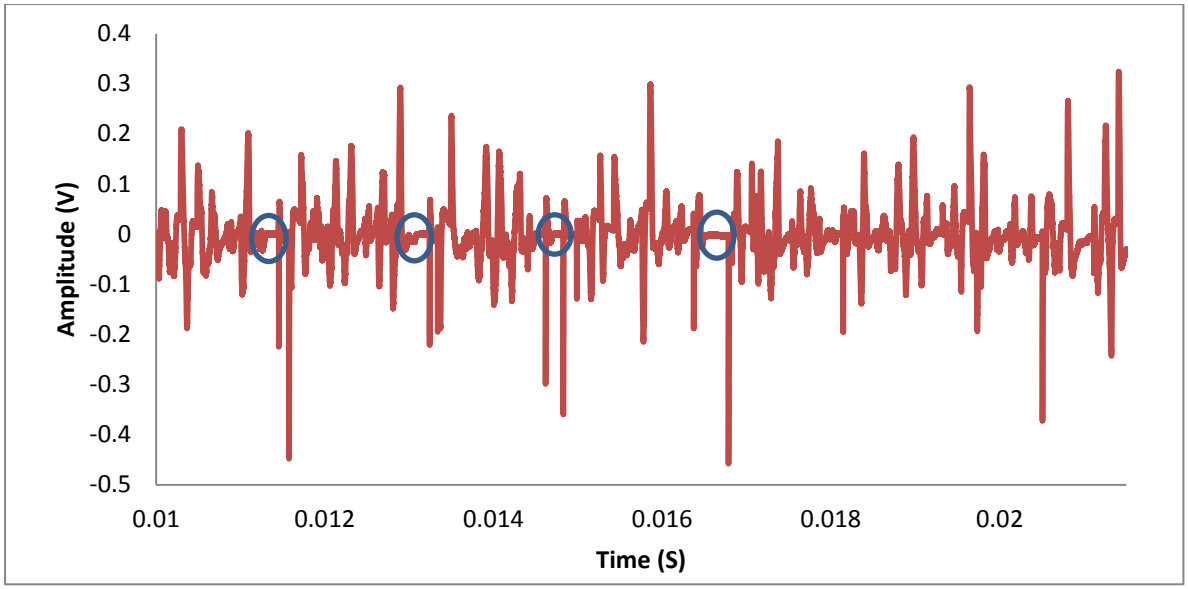

Figure 22 Typical AE time waveform (fault-free condition, 100% maximum continuous power)

Figure 23 (a) shows the AE signature prior to, and after signal separation of the deterministic components. Figure 23 (b) clearly exhibited periodic shocks events that were masked by background noise in the original time trace.

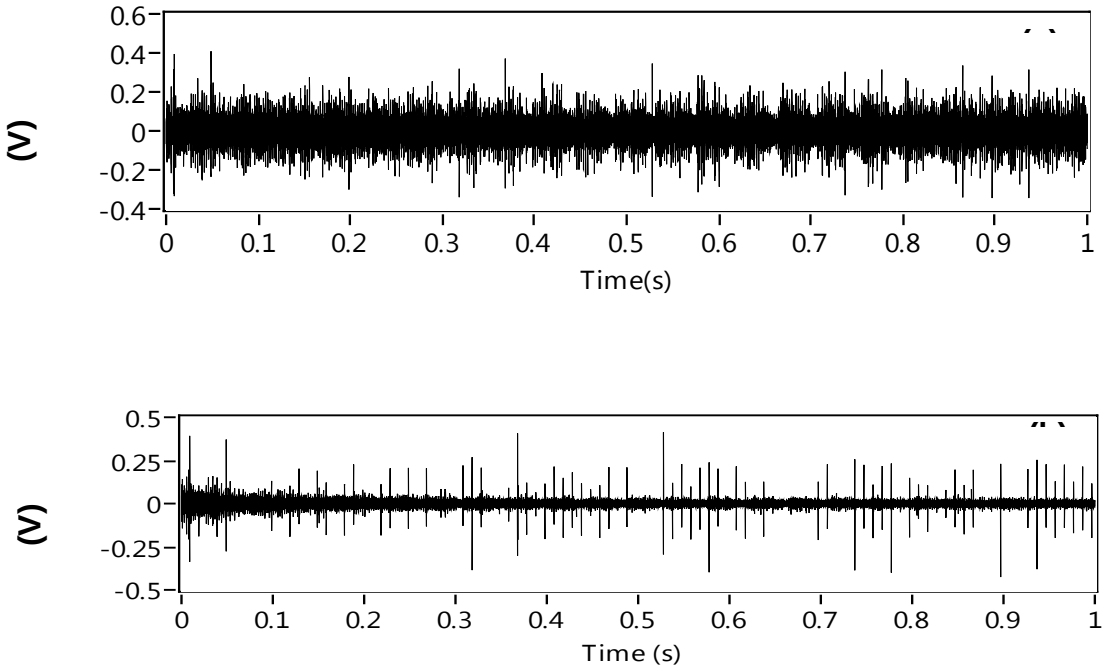

Figure 23 Time waveform of AE signal (a) before and (b) after separation for small defect

The Spectral Kurtosis was employed to extract the filter characteristics which were utilised for envelope analysis on measured AE signatures. Associated typical kurtograms of SK analysis are shown in figure 24. The result of maximum kurtosis showed there were no noticeable differences between healthy and faulty conditions.

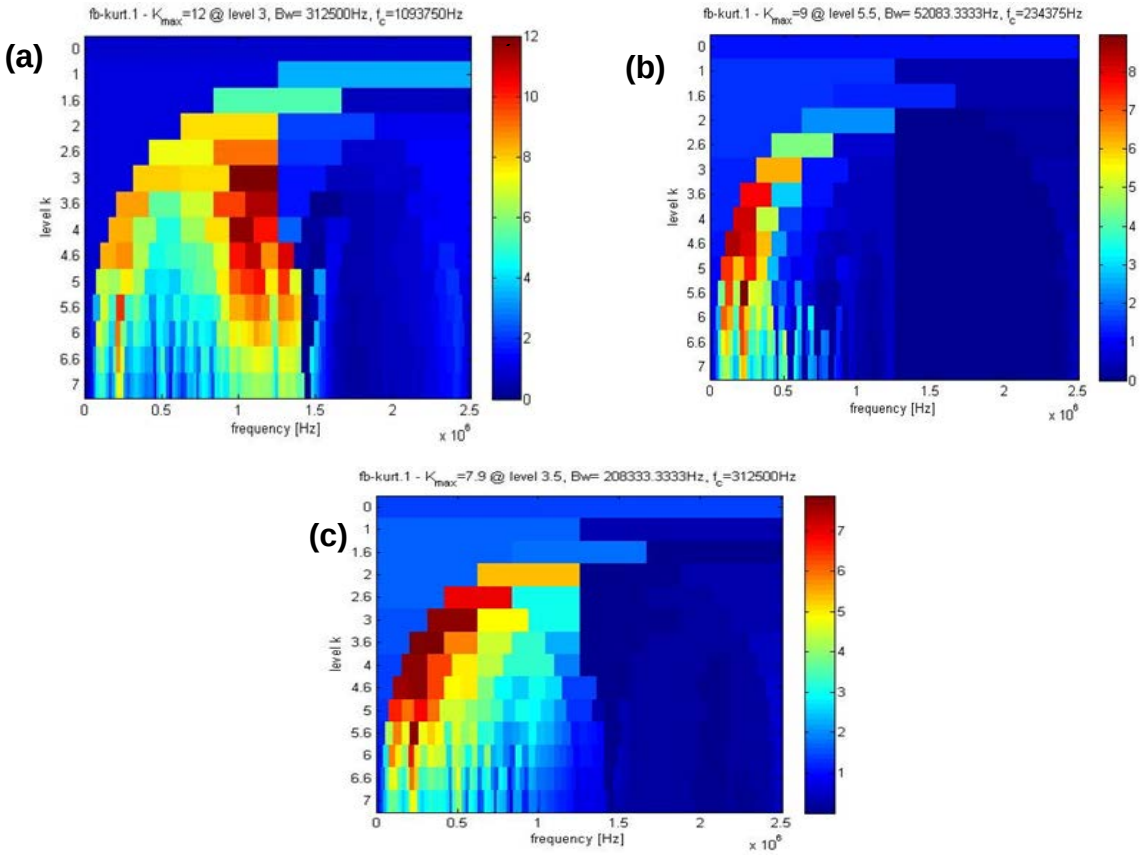

Figure 24 SK kurtograms (a) Fault-free (b) Minor (c) Major defects (110% maximum take-off power)

The envelope analysis was undertaken using the central frequency F_c and bandwidth (Bw) estimated by SK analysis, see table 5. Observations of figures 25, 26 and 27 showed the presence of the bearing outer race defect frequency (96 Hz) and its harmonic (192 Hz) for both minor and major damages under different loading conditions.

Table 5 Filter characteristics estimated based on SK for AE signals

Case	Load condition	Center frequency F_c (Hz)	Band Width (Bw) (Hz)	Kurtosis
Fault-free	110% of maximum take-off power	1093750	312500	12
Minor damage		234375	52083	9
Major damage		312500	208333	7.9
Fault-free	100% of	1093750	312500	12

Minor damage	maximum continuous power	234375	52083	9
Major damage condition		312500	208333	7.9
Fault-free	80 % of maximum continuous power	1093750	312500	12
Minor damage condition		234375	52083	9
Major damage		312500	208333	7.9

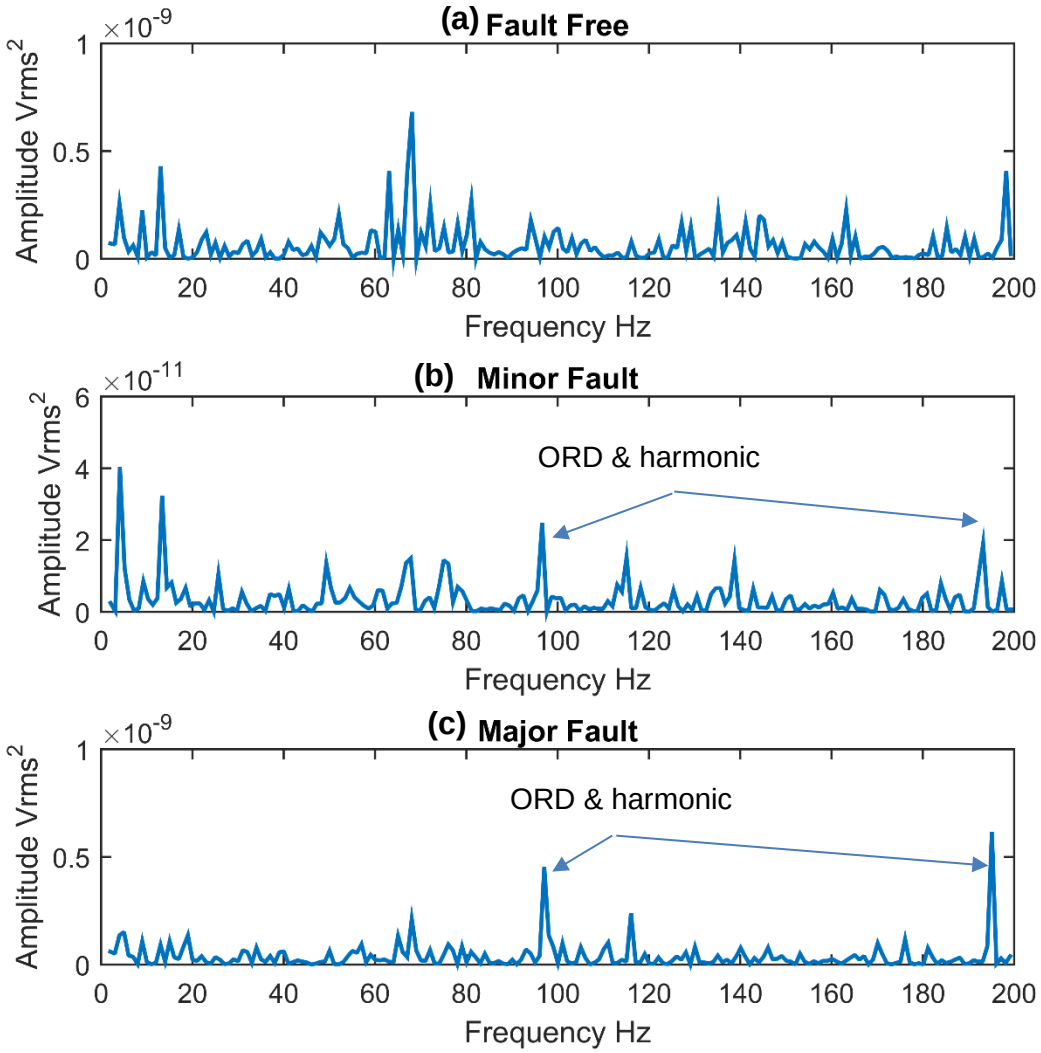

Figure 25 Enveloped spectra of AE signal (a) Fault-free (b) Major (c) Minor bearing defects at 110% maximum take-off power

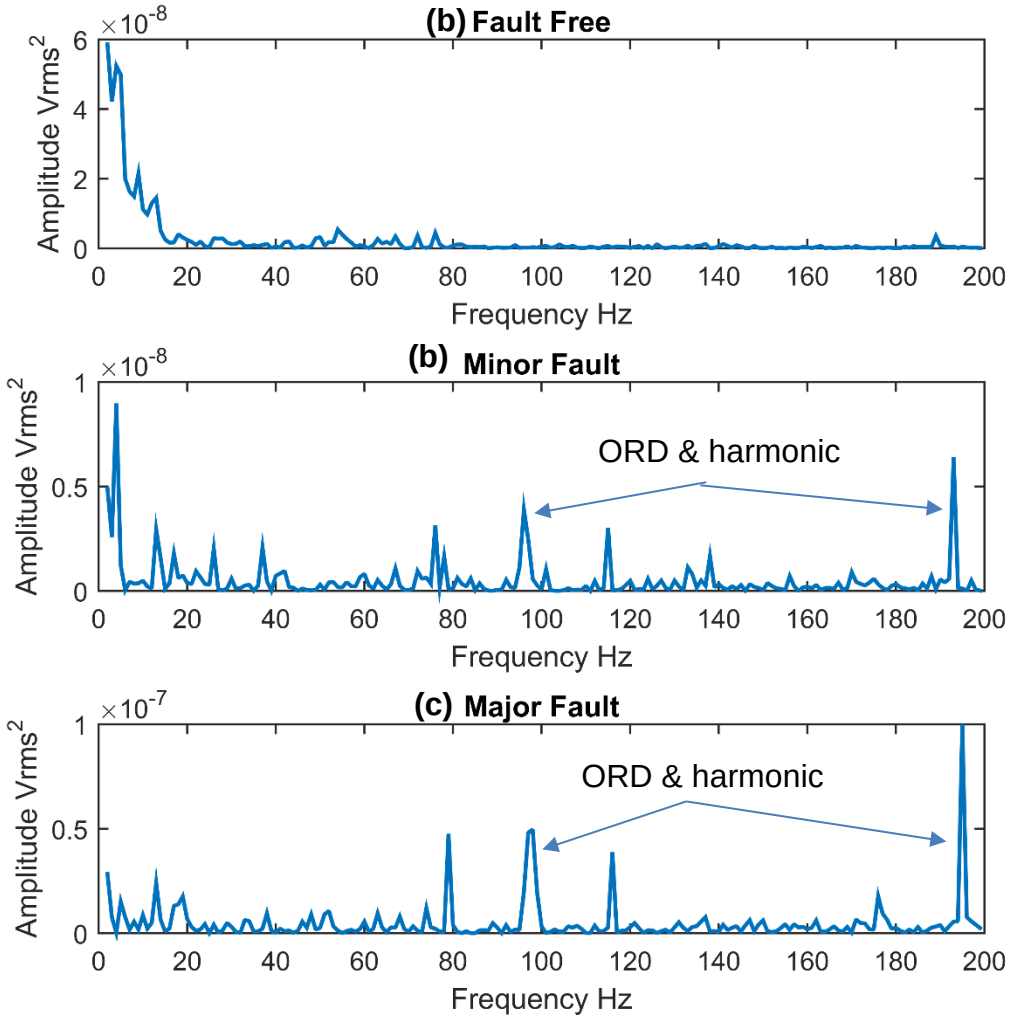

Figure 26 **Enveloped spectra of AE signal (a) Fault-free (b) Major (c) Minor bearing defects at 100% maximum continuous power**

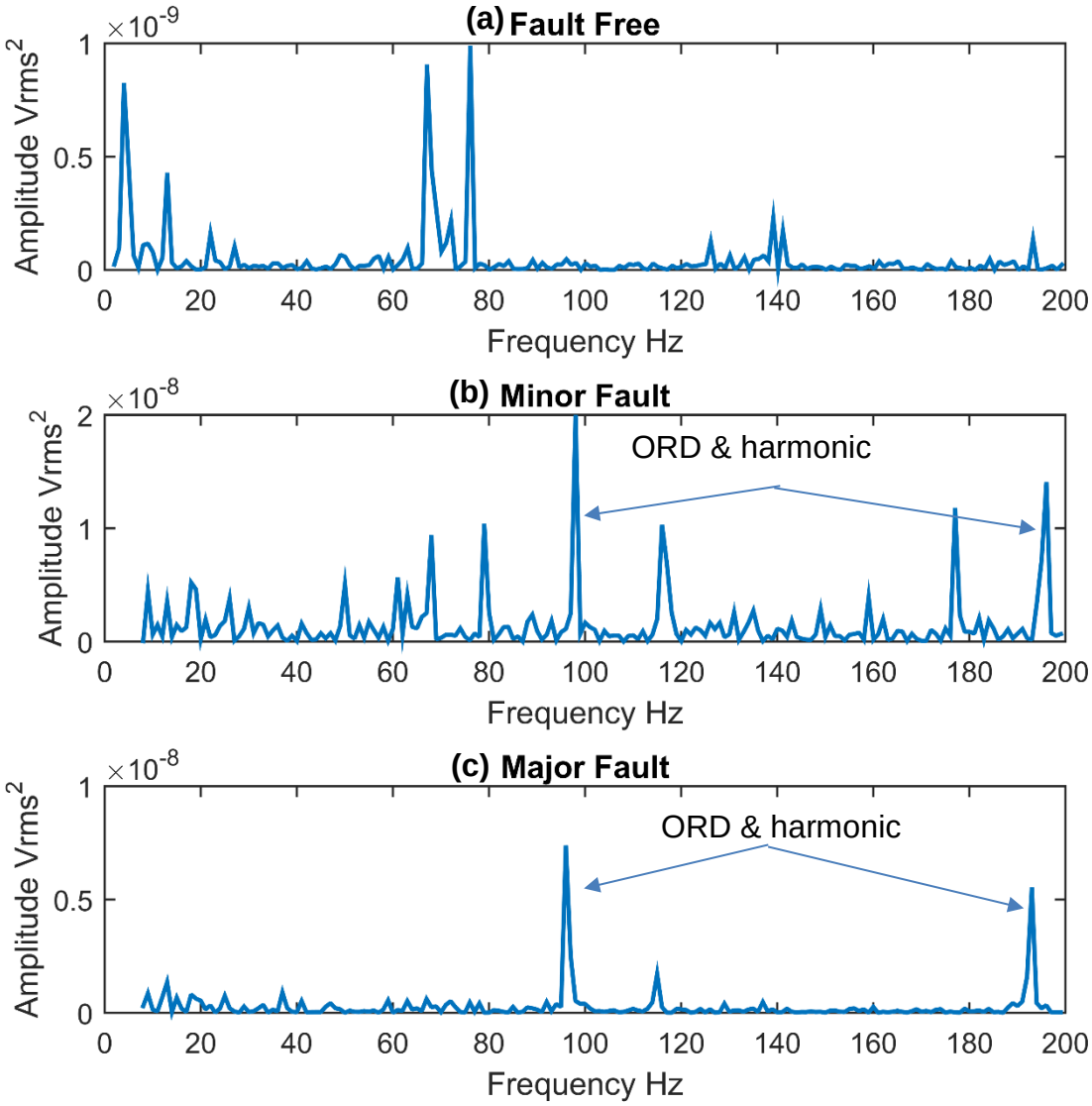

Figure 27 **Enveloped spectra of AE signal (a) Fault-free (b) Minor (c) Major bearing defects at 80% maximum continuous power**

8 Discussion and conclusion

In order to increase the signal to noise level under strong background noise, the AE sensor (PWAS) was attached on the surface of the planet carrier. An advanced wireless transmission system was employed for this investigation. In its current form, the wireless transfer system is only able to support a single sensor, and therefore it was necessary to select a location at which to attach the sensor. The dish of the planet carrier provided ideal location due to the fact that most of helicopters share same design feature of planet carrier. In addition it is the closer part to bearings which are the root cause of the mot gearbox failures.

The acquired AE a signal contains clear peaks at typical gear mesh frequencies showing that a meaningful signal is being transferred from the sensor. Signal energy levels varied enormously with frequency; typical Fourier amplitudes at 10 kHz are four orders of magnitude larger than those at 1 MHz. It is unusual to be able to make these comparisons since many AE sensors are only useful in a limited frequency range. However, the broadband sensitivity of the PWAS sensor also presents challenges since the large energy levels at low frequency which are present within the gearbox can affect the sensor. In addition intermittent AE signal transmission was observed on the signal, this was attributed to the large vibrations impacting on the sensory-side circuitry.

The techniques used in this paper are typically used for applications where strong background noise masks the defect signature of interest within the measured vibration signature. The AE signal is more susceptible to background noise and in this case, the arduous transmission path from the outer race through the rollers to the inner race and then the planet carrier makes the ability to identify outer race defects, even more, challenging. However, the use of the wireless system incorporated into the main gearbox has contributed significantly to improving the signal-to-noise ratio.

A comparison of the vibration and AE analysis showed AE analysis was able to identify the presence of the bearing outer race defect frequency (96 Hz) and its harmonic (192 Hz) for both minor and major damaged for all loading cases based on observations on the enveloped spectra. However, for vibration analysis, the outer race defect for minor damage case was only detected for the 110% the maximum take-off power condition in Y and Z directions. The

inner race defect was not detected by both AE and vibration analysis due to the nature of the inner race fault, as shown in figure 5. Such a distributed fault (natural spalling all around the race) does not generate the theoretical inner race defect frequency due to the absence of singular impacts when bearing rollers/balls passing the inner race..

For the vibration analysis, the measurement taken in X direction showed no fault was identified for the minor damaged condition under all load conditions. In addition, the enveloped spectrum was dominated by the gear mesh frequencies and their harmonics, and as such the bearing defect frequencies were not evident. However, AE analysis was able to identify both the minor and major defect conditions. Detection of the small bearing defect gives the AE an indisputable diagnosis advantage and emphasis the benefit of having sensors embedded with the gearbox.

The ability of applied signal processing techniques to identify the presence of bearing fault is based on removing the masked signal and the identification of particular frequency regions with high impact energy; these impacts are due to the presence of the bearing defect which affects bearing sliding motion. Results of vibration analysis show sensitivity to the direction of vibration measurement.
Vibration analysis showed the fault detection depended on the measurement direction with measurements in Y and Z showing stronger signal components compared to the X direction (vibration signals acquired from the X direction was dominated by the noise). In addition, the fault detection was best for vibration signals acquired under maximum take-off load (110% Load).

In summary, an investigation employing external vibration and internal AE measurements to identify the presence of a bearing defect in a CS-29 ‘Category A’ helicopter main gearbox has been undertaken. A series of signal processing techniques were applied to extract the bearing fault signature, which included an adaptive filter, Spectral Kurtosis, and envelope analysis. The combination of these techniques demonstrated the ability to identify the presence of the various defect sizes of bearing in comparison to a typical frequency spectrum.

From the results presented it was clearly evident that the internal AE sensor offered a much earlier indication of damage compared to the traditional vibration analysis.

Acknowledgements

This work was conducted as part of EASA study 2015.OP.13 into improved detection techniques for helicopter main gearbox defects.

Declaration

The authors declare there is no conflict of interest.

References

1. Chin H, Danai K and Lewicki DG. *Pattern classifier for health monitoring of helicopter gearboxes*. Report no. No. NASA-E-7741.

2. Zakrajsek JJ. A Review of Transmission Diagnostics Research at NASA Lewis Research Center. Report no. ARL-TR-599, NASA-TM-106746, E-9158, NAS 1.15:106746.

3. Chin H, Danai K and Lewicki DG. Efficient fault diagnosis of helicopter gearboxes. (No. NASA-E-7975). NATIONAL AERONAUTICS AND SPACE ADMINISTRATION CLEVELAND OH LEWIS RESEARCH CENTER 1993.

4. Decker HJ.
Crack Detection for Aerospace Quality Spur Gears. Report no. NASA / TM---2002-211492,ARL-TR-2682.

5. Pipe K. Measuring the Performance of a HUM System-the Features that Count. In: *Third International Conference on Health and Usage Monitoring-HUMS2003*Anonymous , pp.5.

6. Samuel PD and Pines DJ. A review of vibration-based techniques for helicopter transmission diagnostics. J Sound Vibrat 2005; 282: 475-508.

7. Decker HJ and Lewicki DG. Spiral Bevel Pinion Crack Detection in a Helicopter Gearbox. Report no. NASA/TM—2003-212327-- ARL–TR–2958.

8. Dempsey PJ, Keller JA and Wade DR. Signal Detection Theory Applied to Helicopter Transmission Diagnostic Thresholds. In: *Proceedings of the American Helicopter Society 65 th Annual Forum on Disc*Anonymous .

9. Cotrell JR. A preliminary evaluation of a multiple-generator drivetrain configuration for wind turbines. In: *ASME 2002 Wind Energy Symposium*Anonymous , pp.345-352: American Society of Mechanical Engineers.

10. Lynwander P. *Gear drive systems: design and application*: CRC Press, 1983.

11. Kahraman A. Planetary gear train dynamics. Journal of Mechanical Design 1994; 116: 713-720.

12. Huang C, Tsai M, Dorrell DG, et al. Development of a magnetic planetary gearbox. Magnetics, IEEE Transactions on 2008; 44: 403-412.

13. P. R. *Dudley's Handbook of Practical Gear Design and Manufacture*. second ed. USA: CRC press, 2012.

14. Bin Lu, Yaoyu Li, Xin Wu, et al. A review of recent advances in wind turbine condition monitoring and fault diagnosis. In: *Power Electronics and Machines in Wind Applications, 2009. PEMWA 2009. IEEE*Anonymous , pp.1-7.

15. McFadden PD. A revised model for the extraction of periodic waveforms by time domain averaging. Mechanical Systems and Signal Processing 1987; 1: 83-95.

16. Randall RB. Detection and diagnosis of incipient bearing failure in helicopter gearboxes. Eng Failure Anal 2004; 11: 177-190.

17. Wang W. Early detection of gear tooth cracking using the resonance demodulation technique. Mechanical Systems and Signal Processing 2001; 15: 887-903.

18. Musial W, Butterfield S and McNiff B. Improving wind turbine gearbox reliability. In: *Proceedings of the European wind energy conference*Anonymous .

19. Department for Transport. Report on the accident to aerospatiale (Eurrocopter) AS332 L2 Super Puma,registration G-REDL 11 nm NE of Peterhead, Scotland, on 1 April 2009 . Report no. 2/2011.

20. McFadden PD and Toozhy MM. Application of Synchronous
Averaging to Vibration Monitoring of rolling elements bearings. Mechanical Systems and Signal Processing 2000; 14: 891-906.

21. Sawalhi N, Randall RB and Forrester D. Separation and enhancement of gear and bearing signals for the diagnosis of wind turbine transmission systems. Wind Energy 2014; 17: 729-743.

22. McFadden PD and Smith JD. Vibration monitoring of rolling element bearings by the high-frequency resonance technique — a review. Tribol Int 1984; 17: 3-10.

23. Yang W, Tavner PJ and Wilkinson MR. Condition monitoring and fault diagnosis of a wind turbine synchronous generator drive train. Renewable Power Generation, IET 2009; 3: 1-11.

24. Wenxian Yang, Tavner PJ, Crabtree CJ, et al. Cost-Effective Condition Monitoring for Wind Turbines. Industrial Electronics, IEEE Transactions on 2010; 57: 263-271.

25. Randall RB, Sawalhi N and Coats M. A comparison of methods for separation of deterministic and random signals. The International Journal of Condition Monitoring 2011; 1: 11.

26. Randall RB and Antoni J. Rolling element bearing diagnostics—A tutorial. Mechanical Systems and Signal Processing 2011; 25: 485-520.

27. Antoni J and Randall RB. optimisation of SANC for Separating gear and bearing signals. Condition monitoring and diagnostics engineering management 2001: 89-99.

28. Ho D and Randall RB. Optimisation of bearing diagnostic techniques using simulated and actual bearing fault signal. Mechanical Systems and Signal Processing 2000; 14: 763-788.

29. Antoni J. Blind separation of vibration components: Principles and demonstrations. Mechanical Systems and Signal Processing 2005; 19: 1166-1180.

30. Li Z, Yan X, Tian Z, et al. Blind vibration component separation and nonlinear feature extraction applied to the nonstationary vibration signals for the gearbox multi-fault diagnosis. Measurement 2013; 46: 259-271.

31. Barszcz T. Decomposition of vibration signals into deterministic and nondeterministic components and its capabilities of fault detection and identification. International Journal of Applied Mathematics and Computer Science 2009; 19: 327-335.

32. Randall RB. *Vibration-based Condition Monitoring*. first ed. UK: John Wiley and sons Ltd, 2011.

33. Wang W. Autoregressive model-based diagnostics for gears and bearings. Insight-Non-Destructive Testing and Condition Monitoring 2008; 50: 414-418.

34. Makhoul J. Linear prediction: A tutorial review. Proceedings of the IEEE 1975; 63: 561-580.

35. Satorius EH, Zeidler JR and Alexander ST. Noise cancellation via linear prediction filtering. In: *Acoustics, Speech, and Signal Processing, IEEE International Conference on ICASSP '79.*Anonymous , pp.937-940.

36. Anonymous .

37. Thakor NV and Zhu Y. Applications of adaptive filtering to ECG analysis: noise cancellation and arrhythmia detection. Biomedical Engineering, IEEE Transactions on 1991; 38: 785-794.

38. Chaturved GK and Thomas DW. Adaptive noise cancelling and condition monitoring. J Sound Vibrat 1981; 76: 391-405.

39. Antoni J and Randall RB. Unsupervised noise cancellation for vibration signals: part I—evaluation of adaptive algorithms. Mechanical Systems and Signal Processing 2004; 18: 89-101.

40. Widrow B, Glover JR, Jr., McCool JM, et al. Adaptive noise cancelling: Principles and applications. Proceedings of the IEEE 1975; 63: 1692-1716.

41. Simon H. *Adaptive Filter theory*. Second ed. USA: Prentice-Hall international, Inc, 1991.

42. Antoni J and Randall R. The spectral kurtosis: application to the vibratory surveillance and diagnostics of rotating machines. Mechanical Systems and Signal Processing 2006; 20: 308-331.

43. Antoni J. Fast computation of the kurtogram for the detection of transient faults. Mechanical Systems and Signal Processing 2007; 21: 108-124.

44. Dwyer R. Detection of non-Gaussian signals by frequency domain kurtosis estimation. In: *Acoustics, Speech, and Signal Processing, IEEE International Conference on ICASSP'83*.Anonymous , pp.607-610: IEEE.

45. Elasha F, Ruiz-Carcel C, Mba D, et al. A Comparative Study of the Effectiveness of Adaptive Filter Algorithms, Spectral Kurtosis and Linear Prediction in Detection of a Naturally Degraded Bearing in a Gearbox. Journal of Failure Analysis and Prevention 2014; 14: 623-636.

46. Holroyd T. Acoustic Emission as a basis for the condition monitoring of industrial machinery. In: *Proceedings of the 18 th Machinery vibration seminar, Canadian Machinery vibration association*Anonymous , pp.27-29.

47. Kilundu B, Chiementin X, Duez J, et al. Cyclostationarity of Acoustic Emissions (AE) for monitoring bearing defects. Mechanical systems and signal Processing 2011; 25: 2061-2072.

48. Ruiz-Cárcel C, Hernani-Ros E, Cao Y, et al. Use of Spectral Kurtosis for Improving Signal to Noise Ratio of Acoustic Emission Signal from Defective Bearings. Journal of Failure Analysis and Prevention 2014; 14: 363-371.

49. Eftekharnejad B, Carrasco M, Charnley B, et al. The application of spectral kurtosis on acoustic emission and vibrations from a defective bearing. Mechanical Systems and Signal Processing 2011; 25: 266-284.

50. Mba D, Bannister R and Findlay G. Condition monitoring of low-speed rotating machinery using stress waves Part 1. Proc Inst Mech Eng Part E J Process Mech Eng 1999; 213: 153-170.

51. Mba D and Rao RB. Development of Acoustic Emission Technology for Condition Monitoring and Diagnosis of Rotating Machines; Bearings, Pumps, Gearboxes, Engines and Rotating Structures. 2006.

52. Tan CK, Irving P and Mba D. A comparative experimental study on the diagnostic and prognostic capabilities of acoustics emission, vibration and spectrometric oil analysis for spur gears. Mechanical Systems and Signal Processing 2007; 21: 208-233.

53. Al-Ghamd AM and Mba D. A comparative experimental study on the use of acoustic emission and vibration analysis for bearing defect identification and estimation of defect size. Mechanical Systems and Signal Processing 2006; 20: 1537-1571.

54. Mba D. Prognostic opportunities offered by acoustic emission for monitoring bearings and gearboxes. In: *Twelfth international congress on sound and vibration*Anonymous .

55. Couturier J and Mba D. Operational bearing parameters and acoustic emission generation. Journal of Vibration and Acoustics 2008; 130: 024502.

56. Sikorska J and Mba D. Challenges and obstacles in the application of acoustic emission to process machinery. Proc Inst Mech Eng Part E J Process Mech Eng 2008; 222: 1-19.

57. Eftekharnejad B and Mba D. Seeded fault detection on helical gears with acoustic emission. Appl Acoust 2009; 70: 547-555.

58. Elforjani M and Mba D. Monitoring the onset and propagation of natural degradation process in a slow speed rolling element bearing with acoustic emission. Journal of Vibration and Acoustics 2008; 130: 041013.

59. Al-Balushi KR, Addali A, Charnley B, et al. Energy Index technique for detection of Acoustic Emissions associated with incipient bearing failures. Appl Acoust 2010; 71: 812-821.

60. Qu Y, Van Hecke B, He D, et al. Gearbox Fault Diagnostics using AE Sensors with Low Sampling Rate. J. Acoustic Emission 2013; 31: 67.

61. Elforjani M, Mba D, Muhammad A, et al. Condition monitoring of worm gears. Appl Acoust 2012; 73: 859-863.

62. Elasha F, Ruiz-Cárcel C, Mba D, et al. Pitting detection in worm gearboxes with vibration analysis. Eng Failure Anal 2014; 42: 366-376.

63. Howard I. A review of rolling element bearing vibration " Detection, Diagnosis and Prognosis". Report no. DSTO-RR-0013.

64. Khemili I and Chouchane M. Detection of rolling element bearing defects by adaptive filtering. European Journal of Mechanics - A/Solids 2005; 24: 293-303.

65. Bonnardot F, El Badaoui M, Randall RB, et al. Use of the acceleration signal of a gearbox in order to perform angular resampling (with limited speed fluctuation). Mechanical Systems and Signal Processing 2005; 19: 766-785.

66. Sait A and Sharaf-Eldeen Y. A Review of Gearbox Condition Monitoring Based on vibration Analysis Techniques Diagnostics and Prognostics. In: Proulx T (ed) *Rotating Machinery, Structural Health Monitoring, Shock and Vibration, Volume 5*: Springer New York, 2011, p.307.

67. Martin H,R. Statistical Moment Analysis as a Means of Surface Damage Detection. Proceeding of the 7th International Model Analysis Conference, Society of Experimental Mechanics 1989: 1016-1021.

68. Mehala N and Dahiya R. A comparative study of FFT, STFT and wavelet techniques for induction machine fault diagnostic analysis. In: *Proceedings of the 7th WSEAS international conference on Computational intelligence, man-machine systems and cybernetics*Anonymous , Cairo, Egypt, pp.203-208. WSEAS; Stevens Point, Wisconsin, USA: World Scientific and Engineering Academy and Society.

69. Wang WJ and McFadden PD. APPLICATION OF WAVELETS TO GEARBOX VIBRATION SIGNALS FOR FAULT DETECTION. J Sound Vibrat 1996; 192: 927-939.

70. Wang WJ and McFadden PD. Early detection of gear failure by vibration analysis i. calculation of the time-frequency distribution. Mechanical Systems and Signal Processing 1993; 7: 193-203.

71. Elasha F, Mba D and Ruiz-Carcel C. A comparative study of adaptive filters in detecting a naturally degraded bearing within a gearbox. Case Studies in Mechanical Systems and Signal Processing 2016; 3: 1-8.

72. Douglas SC. *Introduction to Adaptive Filters*: CRC Press, 1999.

73. Douglas SC and Rupp M. Convergence Issues in the LMS Adaptive Filter. In: Madisetti VK (ed) *The Digital signal processing handbook*. Second ed. Atlanta, USA: CRC press, 1999.

74. Widrow B, McCool J and Ball M. The complex LMS algorithm. Proceedings of the IEEE 1975; 63: 719-720.

75. Alan D. *Handbook of the condition monitoring techaniques and methodology*. First edition ed. London UK: Chapman and Hall, 1998.

76. Sawalhi N, Randall RB and Endo H. The enhancement of fault detection and diagnosis in rolling element bearings using minimum entropy deconvolution combined with spectral kurtosis. Mechanical Systems and Signal Processing 2007; 21: 2616-2633.

77. Yu L, Momeni S, Godinez V, et al. Adaptation of PWAS transducers to acoustic emission sensors. In: *SPIE Smart Structures and Materials Nondestructive Evaluation and Health Monitoring*Anonymous , pp.798327-798327-10: International Society for Optics and Photonics.